POLITECNICO DI TORINO
Repository ISTITUZIONALE

Digitalization of analysis of a concrete block layer using machine learning as a sustainable approach

Original
Digitalization of analysis of a concrete block layer using machine learning as a sustainable approach / Narimani, P., Dehghanpour Abyaneh, M., Mohammad Hosseinzadeh Golabchi, M., Golchin, B., Haque, R., Jamshidi, A.. - In: SUSTAINABILITY. - ISSN 2071-1050. - ELETTRONICO. - 16:17(2024). [10.3390/su16177591]

Availability:
This version is available at: 11583/3009851 since: 2026-04-14T08:54:16Z

Publisher:
Multidisciplinary Digital Publishing Institute (MDPI)

Published
DOI:10.3390/su16177591

Terms of use:

This article is made available under terms and conditions as specified in the corresponding bibliographic description in the repository

Publisher copyright

(Article begins on next page)

26 November 2026

sustainability

MDPI

Article

Digitalization of Analysis of a Concrete Block Layer Using Machine Learning as a Sustainable Approach

Parviz Narimani [1], Mohsen Dehghanpour Abyaneh [2], Marzieh Golabchi [3], Babak Golchin [4], Rezwanul Haque [5] and Ali Jamshidi [5,*]

[1] School of Mechanical Engineering, College of Engineering, University of Tehran, Tehran 7787131587, Iran; parviz.narimani@alumni.ut.ac.ir
[2] Department of Mechanical and Aerospace Engineering (DIMEAS), Politechnico Di Torino, 10129 Torino, Italy; mohsen.dehghanpour@polito.it
[3] Department of Energy (DENERG), Politechnico Di Torino, 10129 Torino, Italy; marzieh.mohammad@polito.it
[4] Department of Civil Engineering, University of Mohaghegh Ardabili, Ardabil 5619911367, Iran; b.golchin@uma.ac.ir
[5] School of Science, Technology and Engineering, University of the Sunshine Coast, Sippy Downs, QLD 4556, Australia; rhaque@usc.edu.au
* Correspondence: ajamshidi@usc.edu.au

Abstract: The concrete block pavement (CBP) system has a surface layer consisting of concrete block pavers and joint sand over a bedding sand layer. The non-homogeneous nature of the surface course of CBP, along with different laying patterns and shapes of block pavers, makes the analysis of CBP cumbersome. In this study, the surface course of CBP was modeled based on the slab action of the block pavers and joint sand, which are connected together in full contact. Four different laying patterns, including herringbone, stretcher, parquet, and square, were modeled using a finite element model. The elastic moduli of the block pavers varied from 2500 MPa to 45,000 MPa, with thicknesses ranging from 60 mm to 120 mm. As a result, modeling of CBP based on slab action can be considered a realistic strategy. In addition, a dataset was created based on quantitative inputs, e.g., elastic modulus and thickness of the block pavers, and qualitative input, i.e., block laying patterns. The approaches of machine learning adopted were support vector regression, Gaussian process regression, single-layer and deep artificial neural networks, and least squares boosting to implement prediction approach based on input and output. The analyses of statistical accuracy of all five machine learning methods showed high accuracy; however, the Gaussian process and deep artificial neural network methods resulted in the most accurate outputs and are recommended for further studies. Based on the machine learning models, digitalization is achieved through the development of simple, user-friendly software for electronic devices in order to perform a preliminary analysis of different laying patterns of CBP. Such a platform may result in less laboratory work and boosts the level of sustainability in concrete block pavement technology.

Keywords: concrete block pavement (CBP); stress analysis; machine learning; artificial neural network; digitalization; digital transformation

check for updates

Citation: Narimani, P.; Abyaneh, M.D.; Golabchi, M.; Golchin, B.; Haque, R.; Jamshidi, A. Digitalization of Analysis of a Concrete Block Layer Using Machine Learning as a Sustainable Approach. *Sustainability* **2024**, *16*, 7591. https://doi.org/10.3390/su16177591

Academic Editor: Syed Minhaj Saleem Kazmi

Received: 21 July 2024
Revised: 22 August 2024
Accepted: 27 August 2024
Published: 2 September 2024

Copyright: © 2024 by the authors. Licensee MDPI, Basel, Switzerland. This article is an open access article distributed under the terms and conditions of the Creative Commons Attribution (CC BY) license (https://creativecommons.org/licenses/by/4.0/).

1. Introduction

Concrete block pavement (CBP) is a commonly used paving system in various transportation infrastructures, from lightly trafficked residential streets to heavy-duty industrial yards, such as ports, stacking container yards, and airports. A CBP system comprises a surface course composed of block pavers 60–120 mm in thickness, laid on a 25–50-mm-thick bedding sand layer resting on a granular, cement, or bituminous-treated base/subbase. There is a 2–5-mm gap between the block pavers, filled with sand, which is called joint sand. The joint sand transmits the stress/strain induced through traffic loading vertically and horizontally. The mechanism of load bearing in CBP is fundamentally different from that

in asphalt and concrete pavement. In other words, the mechanism on an asphalt surface is based on the stiffness coming from bitumen aging and the interlocking between aggregate particles, which is due to roller compaction after laying the mix and the compaction of post-construction by vehicles. In concrete pavements, stiffness generally comes from a set of chemical hydrations of cement with water in the curing period and the interlocking of aggregate particles after vibrating and finishing the surface. Conversely, the mechanism of load bearing in CBP is based on progressive interlocking, which is called lock-up, depending on the block shape, block laying pattern, compaction by roller after block laying, and post-compaction by vehicles. In addition, the direction of traffic has no effect on the performance of asphalt and concrete pavement, while the interlocking of the laid pavers should be perpendicular to the direction of the traffic to achieve the highest structural efficiency in heavy-duty applications, such as in ports [1]. The interlocking achieved by the interaction between the block pavers, joint sand, and bedding sand results in an equivalent elastic modulus of 1500–5500 MPa, depending on the blocks' shape and laying pattern [2]. For example, for design purposes, the initial equivalent elastic modulus of an 80 mm block layer with a 25 mm bedding sand layer is assumed to be at least 2400 MPa, with a Poisson's ratio of 0.30, similar to asphalt [3]. In Sweden, the equivalent elastic modulus is 3000 MPa for the block layer and bedding sand. The elastic modulus of the block layer increases due to lock-up. For example, lock-up increases stiffness after passing a 10,000–15,000 equivalent standard axle [2]. The equivalent elastic modulus of the block layer increases up to 6000 MPa throughout the entire lifespan of the pavement. The various concepts for the structural design of CBP are as follows [4]:

- Modified slab analysis [5]
- Layered elastic analysis [6]
- Finite element analysis [7–9]

Based on these methodologies, software and modeling approaches have been commercially developed (Table 1). Although these computer programs and software are useful for the analysis and structural design of CBP as a composite pavement system, it is still important to train engineers and pavement technologists, which is costly and time-consuming.

Table 1. The software packages used for the modeling, structural design, and analysis of CBP.

Software/Computer Package	Methodology	Country	Reference
LOCKPAVE	Linear elastic layer	Australia	[10]
DesignPave	Linear elastic layer	Australia	[11]
BLKPAVE	Linear elastic layer	China	[12]
REFEM	Linear elastic and FEM	Germany	[13]
CERIB	Linear elastic layer	France	[14]
BLP3D	Linear elastic and FEM	Japan	[15]
NITT BLOCKPAVE	FEM by means of PLAXIS	India	[16]
DELPAVE	FEM and elastic linear	Netherlands	[17]
SAP 2000	FEM and elastic linear	Sri Lanka	[18]
ELMOD 6	Linear elastic layer	UK	[19]
GeoStudio	Linear elastic and FEM	UK	[20]
ANSYS	Linear and non-linear elastic and FEM	Iran	[8]
ABAQUS	Linear elastic and FEM	Iran	[21]
ABAQUS	Linear elastic and FEM	China	[22]

To create a user-friendly platform to provide preliminary outputs for initial engineering judgment, it is necessary to adopt more efficient methodologies in the digitalization

of CBP design. These should be based on sophisticated analytical/mechanistic methods and the principles of the human–machine interface. To feed such platforms, a massive database is required, which should be updated regularly. Furthermore, it is critical that these platforms be straightforward enough for all users with different practical and academic backgrounds and informatic skills. Moreover, the platforms need software that is compatible with different operational systems (e.g., Windows and Macintosh) or different commercial electronic devices available in the market under Android and iOS (e.g., tablet, laptop, iPhone, iPad, etc.). To address this demand, a concept must be proposed for CBP based on the digitalization of various elements using sophisticated approaches, such as machine learning (ML). Figure 1 illustrates the concept of digital transformation designed schematically. The significance of this research is highlighted when such platforms enable pavement engineers and technicians to make in situ judgements without laboratory setups containing different block thicknesses and laying patterns and requiring massive training in a labor-, time-, and cost-effective manner. Another advantage of this method is that most of the procedures and standard guidelines developed are ad hoc-based, which do not consider all the parameters, such as block shape, block size, material properties, and laying patterns. This research combines the modeling of CBP in various laying patterns and material characteristics based on FEM to predict stress and deflection using ML methods, which results in replacing the ad hoc approaches with methods with higher accuracy. In addition, the digitalization using ML approaches paves the way to use advanced methods in the analysis of CBP by pavement engineers and technologists.

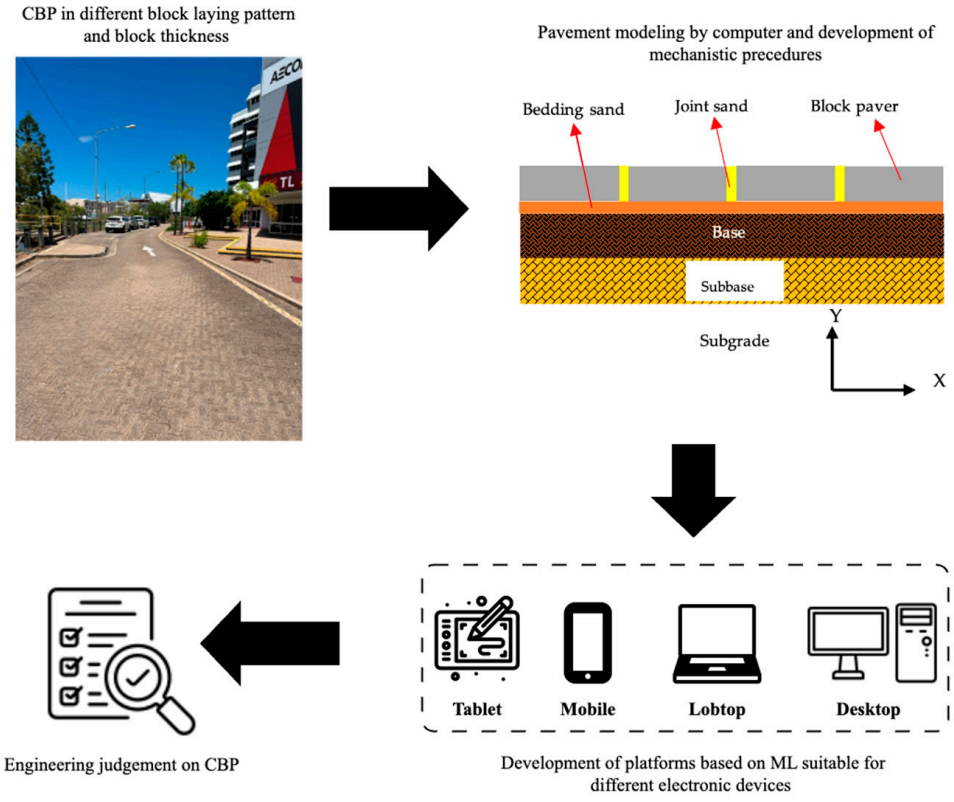


Figure 1. The concept of digital transformation of CBP analysis for a preliminary analysis.

In the field of CBP technology, ML approaches can be used in predictive modeling and maintenance optimization. Although the traditional regression models, such as linear regression, are basic, they struggle to capture complex approaches and data with different trends and non-linear relationships [23]. Recent studies have demonstrated the superiority of ML models like support vector machine, Gaussian process, and random forest (RF) in predicting pavement conditions, outperforming traditional methods by signifi-

cant margins [24]. For instance, RF models have shown a higher accuracy in predicting structural conditions of pavements by 4% [24]. Additionally, some studies have shown that support vector regression (SVR) and artificial neural networks (ANNs) are useful approaches in predicting concrete compressive strength. Furthermore, the results showed that the adoption of appropriate machine learning algorithms can improve the accuracy of the predicting models by up to 93% [25]. Additionally, hybrid models like TransUNet, which combines convolutional neural networks (CNNs) and vision transformers, were effective in block and distress segmentation, showcasing the potential of deep learning in pavement management [26]. It should be noted that the selection of an appropriate machine learning model highly depends on the types (nature) of data. For example, parametric data are especially appropriate for regression, while image data should be analyzed with classification models [27]. Hybrid models are useful for more complex situations, which are beyond the current scope of study. The use of ML approaches with digitalization can result in a new generation of software and computer packages in CBP. The concept of digitalization consists of four stages as follows:

Stage I: Data Collection

In this stage, the laboratory and/or field data of different laying patterns of CBP, block shapes, thicknesses, joint width, base/subbase material, subgrade strength, and traffic loading are collected and processed for simulation and modeling based on FEM and/or elastic linear theory.

Stage II: Computer Simulation/Modeling

In this stage, all the structural components of the CBP system, which is shown in Figure 1, are modeled using the data provided in stage I. The simulation/modeling can be carried out through computer packages or software exclusively developed for CBP, as presented in Table 1. It should be noted that there is no universal model or procedures for modeling CBP. The researchers and engineers can develop any procedures that are consistent with the results of field investigation (ad hoc models), laboratory setups, and previous mechanistic models.

Stage III: ML Models

This stage incorporates a new module into CBP technology. All models and modeling methods can be collected in this module, and predicting models or methods of analysis can be adopted by users. All the models can be run and show results through an application or a user-friendly program installed on a smart phone, either under Android or iOS, on a tablet, or on a personal desktop. In addition, it is feasible to update the database remotely, as the software is cloud-based. In addition, it would be viable to provide data link facilities by developers so that all users could update and/or share data of the new projects.

Stage IV: Engineering Judgement

The engineers, land developers, builders, CBP technologists, and traders are end users and can benefit from this digitalization in the construction industry. It should be noted that such digital platforms or soft infrastructure are just tools to facilitate engineering judgement in a cost-effective manner. Engineering judgement still plays a critical role in the design and construction of CBP.

It is worth mentioning that there are many technologies and procedures to produce environmentally friendly CBP, such as incorporating waste materials into block and base/subbase of permeable block pavement as a multi-role infrastructure [28–33]. However, it is essential to develop soft infrastructure as a platform for further environmentally friendly characteristics. Such digital infrastructure and computer simulation can boost sustainability in the life cycle of infrastructure [34]. Additionally, it should be noted that deep learning was used to develop algorithms for distress detection [26], and an algorithm was proposed to improve the automatic palletization of concrete block pavers on the site [35]. However, there is a lack of research on the use of ML in predicting stress generated by structural loading.

2. Materials and Methods

2.1. Modeling of the Block Layer

The surface layer of CBP is a non-homogenous layer consisting of rigid block pavers connected to each other through joint sand [36]. The block layer is placed on bedding sand lying on a granular or asphalt/cement-treated base, which is similar to the sublayers used in traditional asphalt and concrete pavement (Figure 1). Therefore, the bottleneck of CBP evaluation and analysis is the modeling of the non-homogenous layer in the surface course. In this study, the block layer was modeled based on the slab action of the materials. This means that every block paver is assumed to be a small concrete slab, which transfers load through the width and length of the block. In other words, the slab action of each block distributes/transfers stress and strain induced by traffic in the vertical, horizontal, and torsional directions. In addition, the blocks are connected to each other through slabs made up of sand at the same height as the block pavers. The stiffness of the joint sand is less than that of the pavers. Therefore, block pavers with high stiffness (Slab A and Slab C) are connected together through joint sand, which is modeled as another slab with low stiffness (Slab B), as schematically shown in Figure 2. It is also assumed that the joint sand material is standard, and the joint sand has the same height as the pavers have. Therefore, the thickness of the pavers and joint sand are equal.

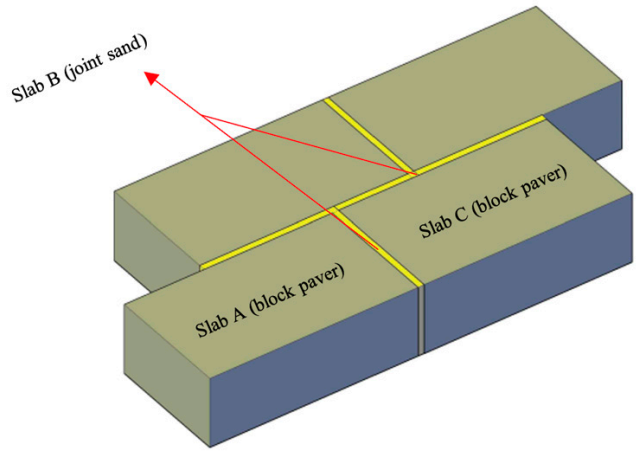


Figure 2. Schematic illustration of modeling CBP using the slab action of the materials.

The advantage of this model is that the vertical load-bearing capacity of the block pavers and joint sand is included in the model, which is more realistic. In addition, the vertical surface of the joint sand is in full contact with the surrounding block pavers, which results in the full transmission of stress/strain to the adjacent blocks and then in the modeling of vertical, horizontal, and torsional interlocking. Figure 3 schematically shows a three-dimensional (3D) image of the CBP modeled based on the slab action of the components in the surface layer. The surface layer consists of a prismatic section in which the material characteristics change over the section from concrete to sand, and vice versa, which results in the non-homogeneous nature of the CBP surface. Another advantage of this modeling is that concrete block pavers and joint sand are assumed to be in full contact with each other. It can be considered as a realistic assumption because the block layer, consisting of the block pavers and joint filling material, is compacted in practice. A high degree of compaction and full contact with the block with a high roughness in narrow spaces of the joints (2–4 mm) make joint (filling) sand material a stiff and impervious medium, which provides shear, rotational, and compressive strength. Therefore, assuming joint sand as networks of slab would not be unrealistic. Furthermore, the total panel of CBP is a slab, which is made of two different materials with an even thickness, i.e., the thickness of the block pavers and joint sand are equal. As a result, the properties of the materials in terms of elastic modulus are not the same, which results in modeling the non-homogeneous nature

of CBP in any software adopted for modeling. Thus, the prismatic and non-homogeneous section deforms under loading as shown in Figure 3. It may be misinterpreted from the schematic in Figure 3 that the tensile stress is induced in the bottom of the joint sand. It should be noted that such stress is not considered in joint sand materials because no binding agent exists. Furthermore, the block layer is laid on the bedding sand layer overlaying the base/subbase layers. The bedding sand layer is in full contact with the joint sand and the block pavers.

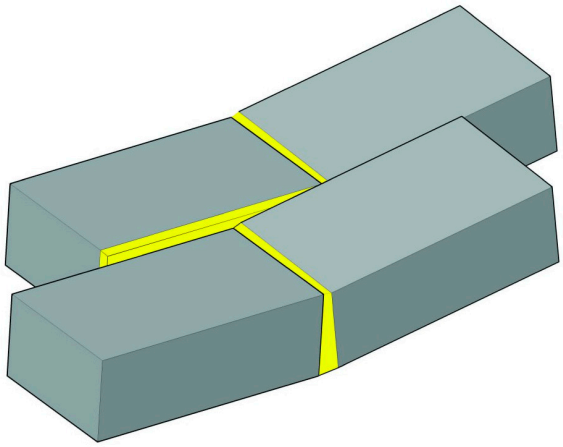
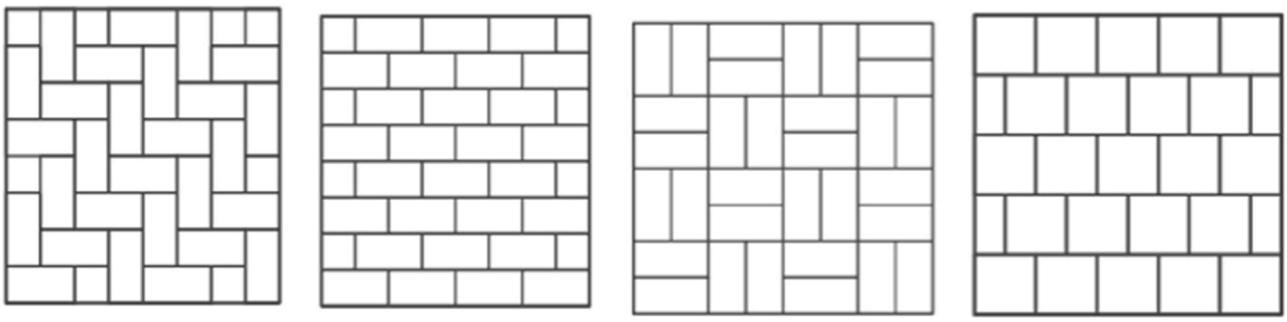


Figure 3. Schematic illustration of the slab action of the pavers and joint sand.

For finite element modeling, Slab Analysis Finite Element (SAFE) software was used. To define the model, the coordination of each corner of the block paver and joints was defined in the software. Panels of 2 m × 2 m in four different laying patterns with rectangular blocks were developed, as shown in Figure 4.



(**a**) Herringbone (**b**) Stretcher (**c**) Parquet (**d**) Square

Figure 4. Different block laying patterns adopted for modeling based on the slab action phenomenon.

2.2. Model Parameters

2.2.1. Inputs

The inputs of the models were the block thicknesses and the elastic modulus of the block and joint sand. Joint sand has the same thickness as concrete block pavers. Table 2 shows the inputs for all the elements. The materials of each slab (i.e., concrete block paver and joint sand) were assigned. Based on the literature, different elastic moduli for concrete block pavers can be adopted, which ranges from 2500 MPa to 45,000 with different thicknesses. To cover all the elastic modulus values, ranging from 2500 MPa to 45,000 MPa, with different thicknesses, were adopted. It is assumed that the standard bedding/joint filling material, i.e., standard size gradation with elastic moduli, was used. The elastic modulus of the subgrade material underlying the base is a rough estimation based on CBR, which is a popular equation in pavement design codes.

Table 2. Model parameters used in computer simulation.

Element	Elastic Modulus (MPa)	Thickness (mm)	Poisson's Ratio
Concrete block paver	2500–45,000	60–120	0.30
Joint sand	350	60–120	0.35
Base layer	225	225	0.35
Subgrade	10 × CBR	---	0.35

2.2.2. Loading

The loading is a single axle load of 8.2 ton at the pavement center. This load was modeled by a 41 kN single wheel load and uniformly distributed over a 270 mm square area, resulting in a 600 kPa contact pressure.

2.2.3. Outputs

The outputs of the model include the stress and deflection beneath the block layer on the base layer of the four different block laying patterns.

2.2.4. Datasets

Given the different laying patterns, 85 elastic moduli, ranging from 2500 MPa to 45,000 MPa at increments of 500 MPa, and four thicknesses, i.e., 60 mm to 120 mm at increments of 20 mm, the total number of input datapoints results in 1360 (4 laying patterns × 4 thicknesses × 85 elastic moduli). Each input has two outputs, stress and deflection under the block layer, which results in 2720 output datapoints. Therefore, the ML models were developed based on 1360 inputs and 2720 outputs.

2.3. ML Algorithm

Data science has rapidly developed and become widely used in pavement engineering analysis, such as pavement performance evaluation, performance prediction, distress recognition, and automatic driving [37–40]. ML methods have shown strong and excellent predictive abilities in this field [41]. The following section introduces three standard ML algorithms that are suitable for the current database structure: regression algorithms based on support vector regression (SVR), Gaussian process regression (GPR), and artificial neural network (ANN). More details are provided below:

2.3.1. SVR

Support vector machines are well-known supervised learning models for solving classification problems [42,43]. SVR aims to simultaneously minimize the empirical risk and maximize the generalization capability of the model [44]. However, this technique is not suitable for regression. To address regression problems, the supported vector regression introduces the concept of an epsilon-insensitive zone. In this method, a margin is defined to control the deviation of the predicted points. The SVR method generally uses a linear function with weights and bias and is trained using nonlinear kernel functions and optimized by standard loss functions developed in various algorithms [45].

2.3.2. GPR

Gaussian process models are non-parametric extensions of linear regression that use Bayesian inference to make probabilistic predictions [46]. The GPR model is a lazy learner, which means that it does not generalize the training data until it receives a query. This differs from other learning algorithms that generalize training data in advance. The GPR model employs a kernel function to measure the similarity between two points and to estimate the value of a new point based on the training data [47]. Furthermore, because Bayesian inference is probabilistic, each prediction has a normal distribution

and a confidence level. These features make GPR suitable for modeling highly nonlinear functions [46].

2.3.3. Single-Layer ANN and Deep ANN

ANN is a popular ML technique that has been applied to various civil engineering problems. It simulates the structure and function of biological neurons in the human brain, which can communicate and process information to form complex concepts and ideas [48,49]. Building a neural network involves three steps: (1) selecting a suitable architecture for the network; (2) training the network with sufficient data; and (3) testing the network with different datasets to evaluate its accuracy. The network consists of weighted connections that indicate the strength of the information flow between the nodes. The weights are adjusted during the training phase to minimize the error between the output and the target values. A single-layer artificial neural network (SANN) consists of one hidden layer, which is suitable for simple and linear problems, while a deep ANN (DANN) has multiple hidden layers and is generally used for complex patterns, modeling, and relationships [50–52]. The network undergoes three phases: training, validation, and testing. The training phase aims to optimize the error function. The validation phase uses the network to construct the model independently from the training phase. The testing phase assesses the performance of the network on unseen data [53].

2.3.4. LSBoost

The least squares boosting method (LSBoost) is an advanced ensemble learning technique used for the development of predictive modeling. It works by sequentially adding weak learners (typically decision trees) to form a strong predictive model. Each new learner is trained to correct the errors made by the previous ones, minimizing the least squares error. This iterative process enhances the model's accuracy and robustness [54]. The LSBoost model involves preparing and pre-processing the data. It should be noted that the LSBoost method starts with a base learner (usually a decision tree) and trains the model iteratively by fitting the base learner to the residuals of the previous model to minimize the least squares error. The model is updated through adding new learners to the ensemble, adjusting weights to correct errors, and then is evaluated using metrics like mean squared error. Fine-tuning the model parameters enhances accuracy and robustness [55]. LSBoost is beneficial for predicting material properties, structural health monitoring, and optimizing construction processes.

2.3.5. Accuracy Metrics

Evaluating metrics is necessary to assess how well an ML regression analysis prediction model performs. Metrics are logical and mathematical constructs that measure how close the predicted outcome is to the actual result [56]. Some of the most commonly used statistics metrics in research are root mean squared error (RMSE), mean absolute percentage error (MAE), mean absolute percentage error (MAPE), and coefficient of determination (R^2) [57]. The RMSE (Equation (1)) measures the dispersion of the residuals and indicates how much the data fits the model. The lower the RMSE value, the better the model. The MAE measures the accuracy of continuous variables without considering the error direction (Equation (2)). Therefore, the MAE is always lower than the RMSE. The MAE also measures the mean error, while the mean percentage error is indicated by MAPE (Equation (3)), which is a metric to evaluate total system error and mean accuracy. The coefficient of determination (R^2) can be interpreted as the proportion of the variance in the dependent variable that is explained by the independent variable [58]. It can range from $-\infty$ to 1; the higher the value, the better (Equation (4)). A recent study [58] has shown that the coefficient of determination (R^2) is more relevant than the other statistical indicators, such as RMSE,

MAE, and MAPE, and that it is better to incorporate it with standard metrics to obtain more realistic judgments.

$$RMSE = \sqrt{\frac{1}{n}\sum_{1}^{n}\left(Y_{pre} - Y_{act}\right)^2} \quad (1)$$

$$MAE = \frac{1}{n}\sum_{1}^{n}\left|Y_{pre} - Y_{act}\right| \quad (2)$$

$$MAPE = \frac{1}{n}\sum_{1}^{n}\frac{\left|Y_{pre} - Y_{act}\right|}{Y_{act}} \times 100 \quad (3)$$

$$R^2 = 1 - \frac{\sum_{1}^{n}\left(Y_{pre} - \overline{Y}_{pre}\right)^2}{\sum_{1}^{n}\left(Y_{act} - \overline{Y}_{act}\right)^2} \quad (4)$$

where Y_{act} is the actual value of the output result from the dataset, Y_{pre} is the predicted value from any machine learning algorithm, $\overline{Y}_{act}$ is the mean value of the actual output, and $\overline{Y}_{pre}$ is the mean value of the predicted output.

2.3.6. Taylor Diagram

A Taylor diagram provides a graphical method to assess the accuracy of various ap-proximate models or the representations of a system, process, or phenomenon. A Taylor diagram incorporates three key statistical measures into a single, straightforward visual format [59]: the centered root mean square difference (CRMSD), the Pearson correlation coefficient, and standard deviations. By doing so, Taylor diagrams facilitate the comparison of different models' relative strengths or the evaluation of changes in a model's performance over time. The CRMSD metric within a Taylor diagram signifies the model's prediction error [56]. It should be noted that all the data presented are from optimized models of the ML approaches. The optimization was carried out using the Bayesian approach and by pre-processing the dataset, such as input normalization, which is automatically handled during each method's implementation.

2.4. Analysis of Sustainability

One of the advantages of digitalization and the use of ML is sustainability. The rate of sustainability can be measured through different approaches, depending on the criteria targeted in the analysis. It is cumbersome to consider all the details in analysis because the energy consumption and global potential warming, in terms of greenhouse gas (GHG) emissions and other contaminants, cannot be readily measured. Additionally, the raw material processing, construction technology, construction method, and recycling technology (if it exists) can be significantly different in paving projects. There are computer packages, such as SIMAPRO [60–62], Gabi Professional Software [63], PaLATE [64], DuboCalc [65], ECORCE [66], VTTI/UC [65], and BEES [67], that analyze the sustainability of different types of pavements based on various parameters and methodologies. It should be noted that the outputs from these computer packages might be inconsistent. However, the resultant trends can be comparable.

In this study, sustainability is analyzed through the evaluation of energy requirements and GHG emissions in raw material processing and block paver production for 2 m × 2 m laboratory setups that were modeled based on slab action. Concrete block paver production consists of eight stages as follows:

- Raw material processing (mining aggregate particles, cement production, water production/processing)
- Mixing the materials
- Pouring the mixtures in the molds
- Compressing the mixture

- Vibrating the mixture
- Shadow/sun drying/curing, depending on the construction method and technology
- Finishing
- Packaging

The mass of concrete for block paver manufacturing in different block laying patterns and the mass of joint sand/bedding sand used in the laboratory models were estimated. Then, energy requirements and GHG emissions were calculated based on the mass of raw materials. The energy requirements for raw material processing and other stages are shown in Table 3. It should be noted that finishing and packaging are out of the scope of this study. The base layer and the compacting energy after laying the blocks are not considered in the analysis of sustainability because these are identical for all the block laying patterns.

Table 3. Energy requirements for raw material processing and construction.

CBP Element	Stage	Material	Energy	Unit	Reference
Block paver	Raw material	Aggregate	53	MJ/ton	[68]
		Cement	6.36	GJ/ton	[69]
		Water	0.473	kwh/m^3	[70]
		Sand	53	MJ/ton	[68]
	Mixing		4.10	MJ/m^3	[71]
	Compressing and vibrating		2.05	MJ/m^3	[71]
	Curing		112	MJ/m^3	[71]
Joint/bedding material	Raw material	Sand	53	MJ/ton	[68]

It is assumed that the industrial fuel is natural gas (NG), and the conversion factor of 1 cubic meter of NG is 38.62 MJ [72]. The calculated GHGs were CO_2, CH_4, and NO_X with conversion factors of 2.023 kgCO_2/unit, 0.003 kgCO_2/unit, and 0.0012 kgCO_2/unit, respectively [73]. The steps for calculating energy requirements and GHG emissions are presented in the flowchart in Figure 5.

It was also assumed that the stages listed below were carried out manually. Therefore, no energy requirement and GHG emissions were calculated:

- Spreading and leveling the bedding sand layer
- Placing different block pavers in each of the laying patterns
- Spreading joint filling sand and brooming into the joints
- Compaction of the block layer by tamper

The mix design ratio of the block pavers was 1 (cement):2 (sand):4 (chip stone), and the water to cement ratio is 0.65, based on the data provided by local manufacturers.

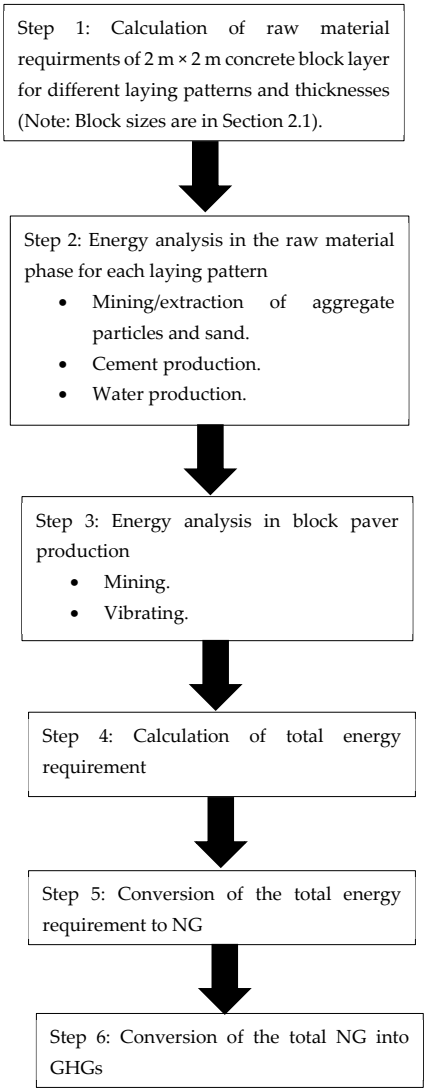


Figure 5. Flowchart of analysis of sustainability (note: the block sizes are in the Section 2.1).

2.5. Digitalization

The digitalization process includes two distinct parts, which are called front-end and back-end. The front-end is a user interface (UI) that interacts with the user and includes a graphical application with text boxes, images, and buttons to provide easy of access for functioning. The second part is the back-end, which is the core of the program and comprises all the appropriate ML models modified during the current investigation. Within the program core, there is a dataset that provides the learning schema in each calculation process. The interface, or front-end, was programmed with MATLAB® (version 2024a) GUI Builder, which is a distinct application within the MATLAB® environment. The back-end was also programmed with the MATLAB® programming language, and the connection between the two (front-end and back-end) was facilitated through inside handles. Additionally, graphical design was provided using free online graphic tools like Canva®, Sydney, Australia, to create a better interface.

2.6. Structure of Study

This study is a multi-disciplinary research project that consists of four fields, as shown in Figure 6. In other words, this paper is the interface between pavement modelling, digitalization, sustainability, and machine learning. It should be noted that the future of pavement analysis and design may integrate data science and information technology.

Therefore, it is necessary to consider information technology as a new approach to maximize sustainability in pavement engineering.

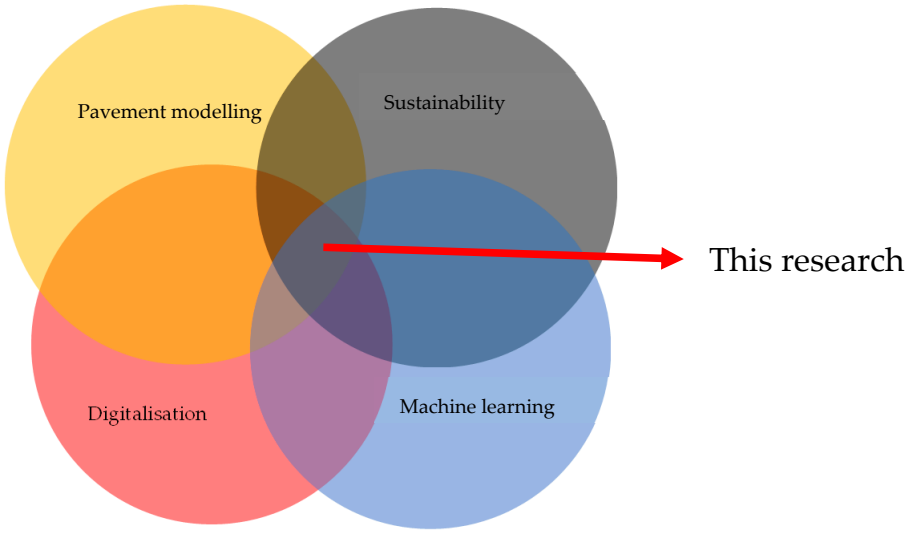


Figure 6. The fields covered in the study.

To carry out the research, the current study consisted of four distinct parts, which are illustrated in Figure 7. The first part (data preprocessing) involves reading data, converting qualitative inputs to quantitative (block laying pattern), and splitting the data into training and testing groups. The second and third parts include the development of the ML model, optimization algorithm, and analysis. The digitalization of ML models is executed in Sections 2 and 3. The last part is the analysis of sustainability.

It should be noted that ML approaches are merely tools adopted to train models based on the data from paving systems modeled through SAFE. In other words, the outputs of the structural models of the CBP based on slab action are trained using ML approaches and are considered as models that can be used for digitalization.

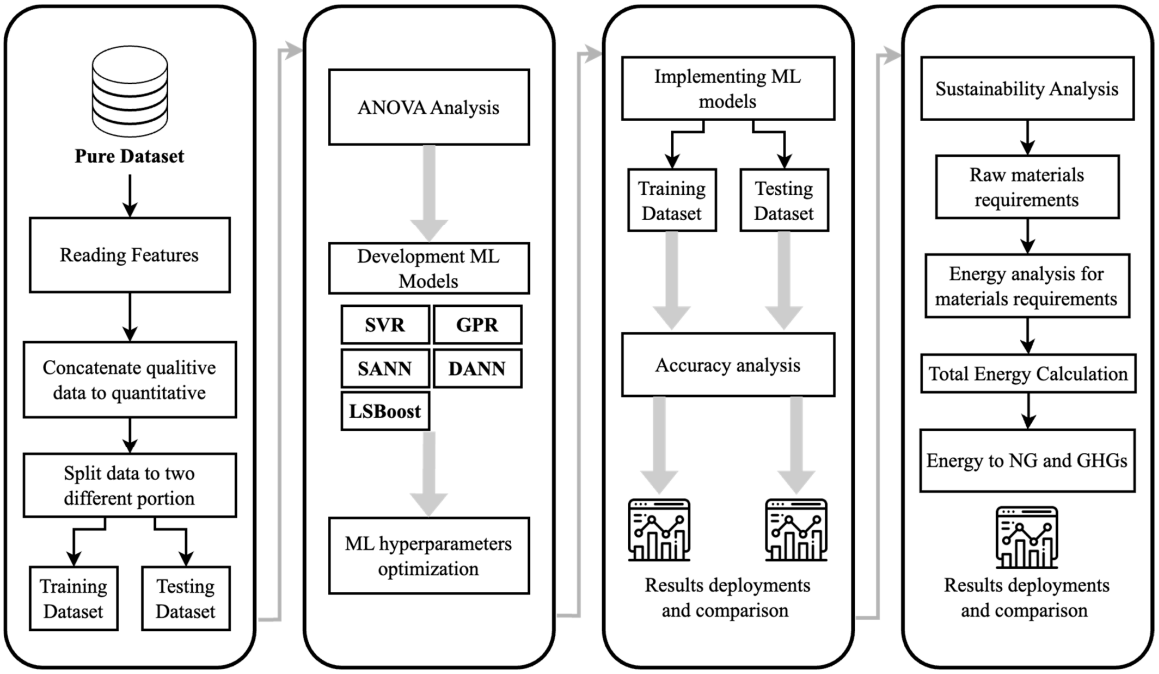


Figure 7. The study procedure schema.

3. Results and Discussion

3.1. Verification

The output of the CBP model, which is based on the slab action of a block layer and joint sand, was compared with a laboratory model tested by Shackel [74]. The contact stress was 600 KPa in the setup, which is the same stress used in the model. The block sizes in the setup were 200 mm × 100 mm × 80 mm. For validation of the model, the same block sizes were used. Table 4 shows the material properties used in the laboratory.

Table 4. Model parameters used in the laboratory [74].

Element	Elastic Modulus (MPa)	Poisson's Ratio
Concrete block paver	2500	0.30
Joint sand	350	0.35
Base layer	225	0.35
Subgrade	225	0.35

The same material properties were used in the model developed by SAFE. The outputs of the model were compared with another FEM developed through ANSYS by Nejad [8] as a case study (Figure 8). It should be noted that the stresses are the maximum stress induced under the center of loading plate beneath the block layer.

As shown in Figure 8, the results are comparable, specifically for the block layer. The block layer decreases the contact stress to 300 MPa, which is half of the load induced, consistent with the stress generated in Shackel's laboratory testing [38]. It is also consistent with Eisenman and Leykauf's outputs, showing that the surface layer decreases the load by approximately 50% [75]. However, there was no data for other elastic moduli for comparison. The reason is that it is labor intensive and costly to produce laboratory setups with block pavers with 2500–45,000 MPa, as mix design and aggregate gradation of blocks are required to be changed to achieve the target elastic moduli. Such a setup would also require 85 tests with increments of 500 MPa. Therefore, this study focused only on the block layer. Figures 9–13 show the effects of the laying pattern block and block shape in terms of the stress and deflection generated under the block layer. It is clear from Figures 9–13 that in every approach, both deflection and stress decreased as thickness increased, which is consisted with field and laboratory data reported by Sun [12]. Additionally, in all methods, the lowest stress and deflection generated under the block layer are in a herringbone laying pattern. Based on the slab action model and ML methods presented in Figures 9–13, the herringbone laying pattern performs better than other methods due to better interlocking, which is consistent with the literature [1,2,18,76–79]. The slab action methodology adopted in the modeling of CBP can simulate torsional, vertical, and horizontal interlocking. Figures 9–13 also show that the worst laying pattern in terms of stress/deflection is the parquet pattern because of the highest stress and deflection generated beneath the block layer. Although the area of the square block (Figure 10a) is the same as that of rectangular block pavers, it performs better than the parquet model. For example, the stress created under the 100 mm block layer of a parquet model using GPR is 303 KPa, while the corresponding values for the parquet and stretcher laying patterns are around 310 KPa, which is almost 3% higher than that of the square pattern for one cycle of loading. A similar trend can be seen in all the block laying patterns and different ML methods used in this study. There are millions of repetitions of traffic loading in reality. Moreover, the stress/deflection under the block layer decreases as the thickness of the block pavers increases, which is consistent with the trend found in the laboratory data reported by Panda and Ghosh [80] and Lin et al. [81]. Therefore, the load-transferring and load-bearing capacities of CBP can be improved as the thickness increases.

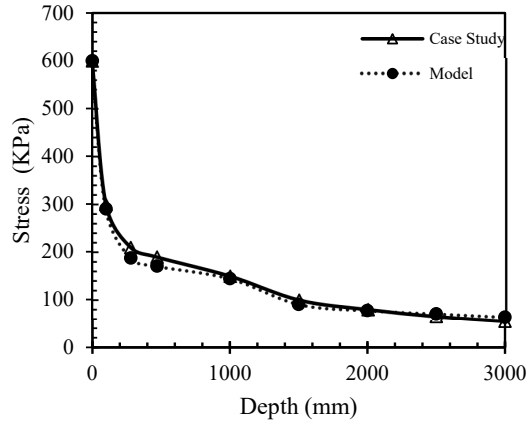


Figure 8. Comparison of the results of the model developed based on slab action of the block layer and a case study.

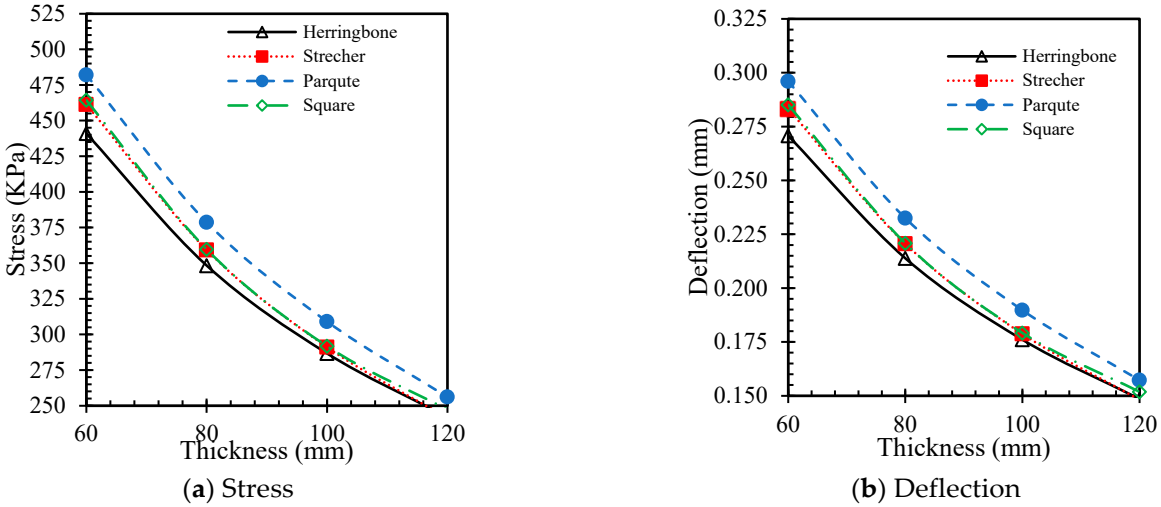


Figure 9. Stress/deflection beneath the block layer thickness: comparison results using the SVR method.

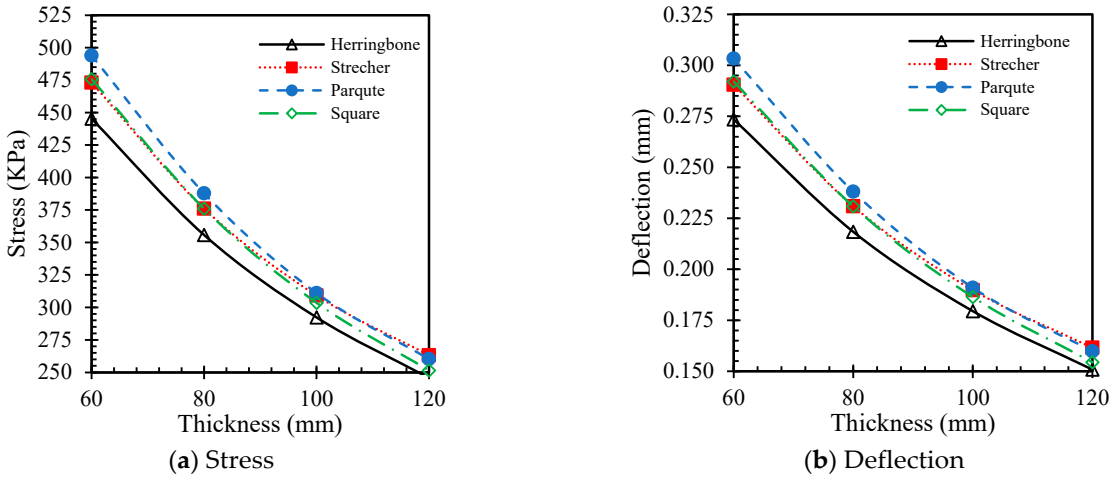
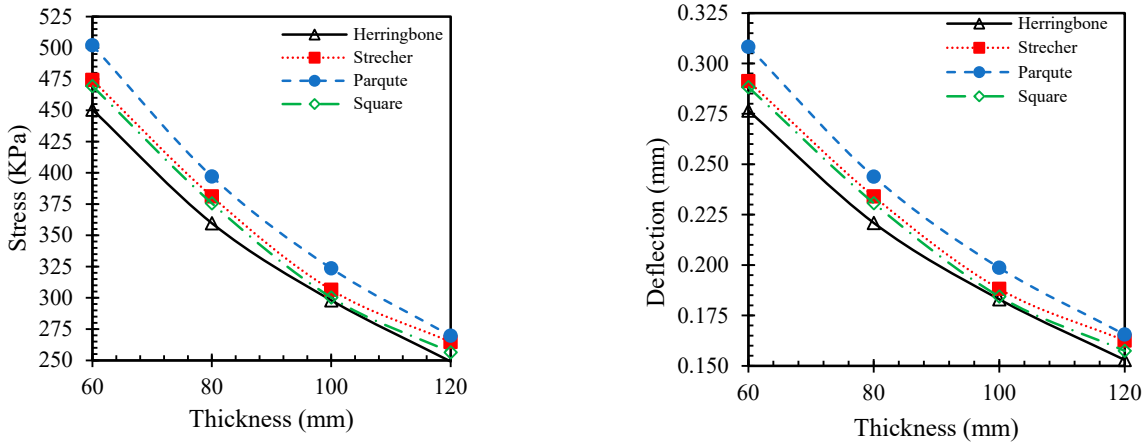
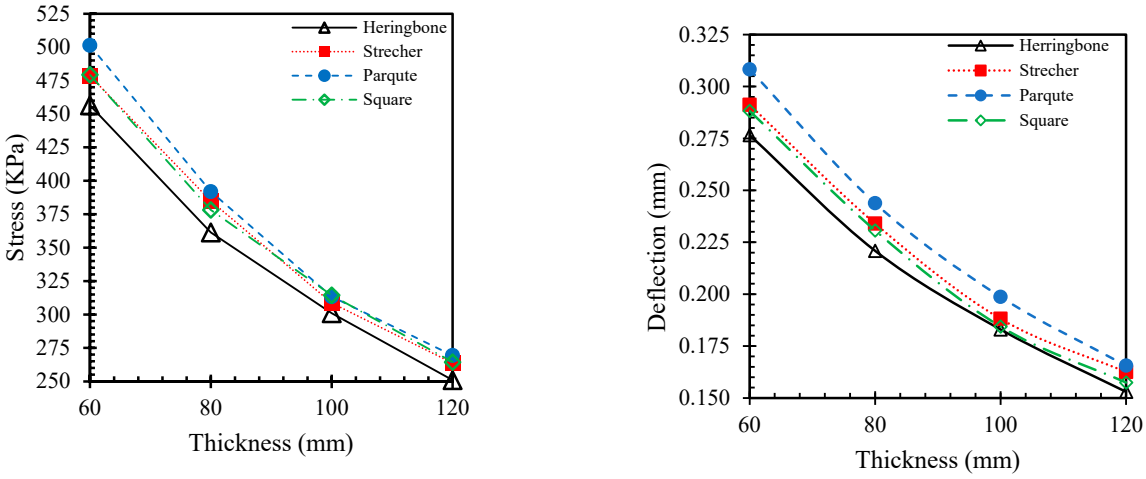


Figure 10. Stress/deflection beneath the block layer thickness: comparison results using the GPR method.



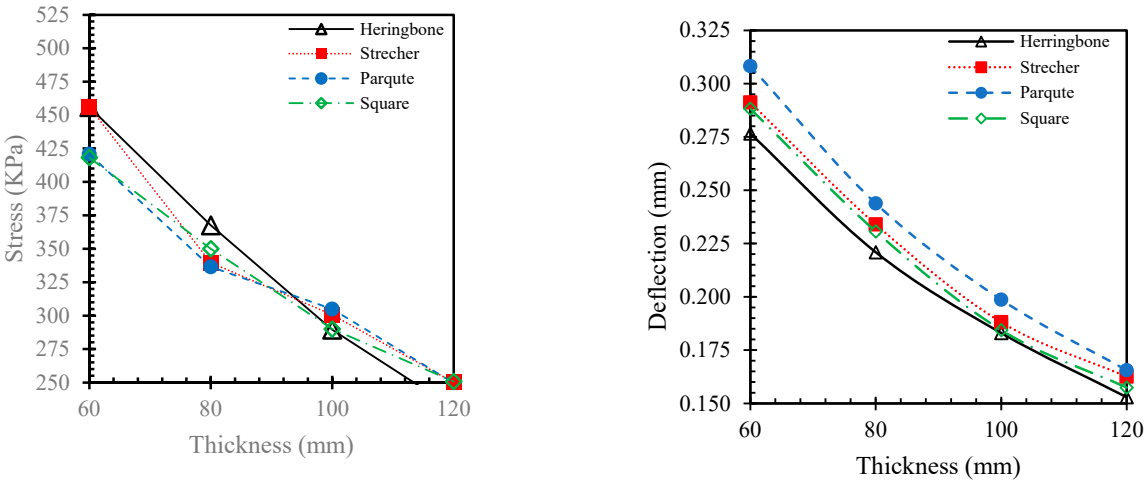
(**a**) Stress (**b**) Deflection

Figure 11. Stress/deflection beneath the block layer thickness: comparison results using the SANN method.



(**a**) Stress (**b**) Deflection

Figure 12. Stress/deflection beneath the block layer: comparison results using the DANN method.



(**a**) Stress (**b**) Deflection

Figure 13. Stress/deflection beneath the block layer: comparison results using the LSBoost method.

3.2. ANOVA

To investigate the effects of different parameters on the overall results (in this case, stress), an ANOVA was performed using a nonlinear regression analysis (Table 5). In the first stage, the qualitative parameters (block laying pattern) were converted into quantitative parameters. There were four different block laying patterns, and each was assigned a natural number between 1 and 4 to indicate the types of concrete block pavement. Table 5 shows the results of the stress test and the corresponding ANOVA.

Table 5. Final results of the ANOVA implementation on the current dataset.

Parameter	Sum sq	df	Mean sq	F	*p*-Value	Description *
Laying pattern	126,885	3	42,295	307	$2.6 \times 10^{-5} < 5\%$	Significant
Thickness	524,823	3	1,806,941	13,119	$5.8 \times 10^{-3} < 5\%$	Significant
E	2,761,950	85	32,496	236	$7 \times 10^{-8} < 5\%$	Significant
Error	176,851	1284	137	-	-	
Total	8,486,511	1375	-	-	-	

* Less than 5% means statistically significant factor.

Table 5 also shows that all the input parameters, including laying pattern, thickness, and elastic modulus of concrete block pavers, have a significant and sensitive effect on the final stress and deflection as the outputs. This means that all the input parameters play a significant role simultaneously. This means that the parameters without a significant role may result in noise in the model, which may decrease the accuracy and predictivity of the model. However, the dynamics governing stress are very complex, and analytical approaches and mathematical models may not capture all aspects of stress, especially when a new parameter, such as block type, is involved in the study. Therefore, the ANOVA test alone cannot reveal the dependence of all the parameters and may require more complex investigations, such as advanced mathematical and ML approaches. The practical approach shows that the surface stress is sensitive to the parameters confirmed by ANOVA, but it does not provide enough correlation about the effects of all parameters on the final results. Thus, in this study, all the parameters were chosen for training the model in ML.

3.3. ML

To apply the three different ML algorithms, the dataset was split into two groups. The first group, which had a large amount of data, was used for training. The second group, which had a small amount of data, was used for validating the algorithms. The validation group had the following properties: (1) block laying patterns, (2) thickness of 60–120 mm, and (3) elastic modulus of 2500–45,000 MPa. The training and testing data had different statistical variety to ensure that the data-splitting procedure worked well and that the data had an appropriate distribution (Table 6).

Table 6. The statistical description of input and output for training and testing datasets.

Variable Name		Min		Max		Average	
		Train	Test	Train	Test	Train	Test
Input	Block Type	1	1	4	4	2.5	2.6
	Thickness (mm)	60	60	120	80	90.36	74.67
	Modulus of Elasticity (MPa)	2500	2500	45,000	41,000	23,815.48	22,216.67
Output	Stress	0.0664	216.33	500.04	368.55	213.12	261.07

Each ML model uses hyperparameters in the main process to determine the final results. Tuning the best hyperparameters can improve the performance of ML models

in the training process. This study optimized the hyperparameters using the Bayesian optimization method, which was implemented using the standard rules of MATLAB® software. The final results are presented in Table 6. In this study, the selection of the next set of hyperparameters was guided by analyzing the posterior function. The function combines a prior distribution (in this specific case, performance metrics of five-fold cross-validation) with known sample data (performance metrics derived from hyperparameters generated at random). By maximizing this posterior information, this study systematically determined the subsequent combination of hyperparameters. This iterative process continued until a predefined criterion was met, and the optimal solution was determined based on the accumulated data of solution samples. Consequently, the hyperparameters for each machine learning model in the study were fine-tuned using Bayesian optimization [82].

Before training any ML algorithm, the optimal hyperparameters were determined using standard Bayesian optimization with five-fold cross-validation. However, each model had many hyperparameters, so tuning all the models would be a time-consuming process. Therefore, this study only optimized several critical hyperparameters, and the remaining hyperparameters were the default values from the MATLAB® software package (Table 7). For the SVR model, the regularization parameter (C), epsilon, and type of kernel function were optimized. The C parameter calculated the degree of penalty for the data points that did not lie within the region. The epsilon parameter allowed an indifference margin around the regression in which a deviation was not counted as an error. The type of kernel function generally controlled the flexibility of the fitting function. For the GPR model, the sigma parameter of the squared exponential kernel and the type of kernel covariance function were optimized. The kernel covariance function could be chosen from a variety of options: rational quadratic (RQ), squared exponential (SE), Matern kernel with parameter 5/2 (M52), and exponential (Exp). These options defined the flexibility of the model to better fit the input data. For the SANN and DANN models, the number of hidden layers, the total number of neurons in each hidden layer, learning rate, and activation function were optimized. The main difference between the single layer and the deep model ANN is the number of hidden layers. This means that the single layer model has one option, while the deep model has more options in the number of layers. Therefore, the deep layer ANN model may perform better in more complex problems. The number of neurons in each layer is another pivotal factor that can improve the efficiency of the model. Although increasing the number of hidden layers and neurons in each layer may enhance the performance of the ANN models, it may contribute to overfitting. Additionally, the learning rate is another essential factor that influences the speed of the learning algorithm to achieve the appropriate weights. In the LSBoost model, the number of learning cycles determines the number of iterations. This means that the more cycles undertaken, the more accurate outcomes from the model, even though there is still a high risk of overfitting. The learning rate influences the contribution of each tree to the final model. A slower learning rate requires more learning cycles, and the maximum split determines the maximum number of splits (or nodes) in each regression tree. More splits can capture more complex patterns but may also increase the potential for overfitting.

Table 7. Hyperparameters' search spaces and their optimal values as determined by Bayesian optimization.

ML Models	Hyperparameters	Search Space	Optimal Values
SVR	C	(0.1, 1000)	84.53
	Epsilon	(0.01, 10)	8.5
	Kernel function	polynomial, Gaussian	polynomial
GPR	Sigma	(0.01, 10)	4.3
	Kernel function	RQ, SE, M52, Exp.	RQ
SANN	Hidden layers	1	1
	Neurons in each layer	(5, 20)	10
	Learning rate	(0.01, 1)	0.1
	Activation function	Relu, Sigmoid, tanh	Relu
DANN	Hidden layers	(2, 20)	3
	Neurons in each layer	(5, 20)	[5, 5, 5]
	Learning rate	(0.01, 1)	0.1
	Activation function	Relu, Sigmoid, tanh	Relu
LSBoost	Number of Learning Cycles	(2, 200)	100
	Maximum Number of Splits	(1, 100)	50
	Learning Rate	(0, 1)	0.1

After performing 1000 iterations for each hyperparameter and comparing the R^2 values as a validation criterion, each model was trained on 1344 datapoints. The training results and their correlations are illustrated in Figures 14–18 for SVR, GPR, SANN, DANN, and LSBoost, respectively. The accuracy metrics, including R^2 for each model, were calculated and showed that all five models had acceptable R^2 values above 0.90, indicating that these models, with the current hyperparameter selection, were suitable for testing new data.

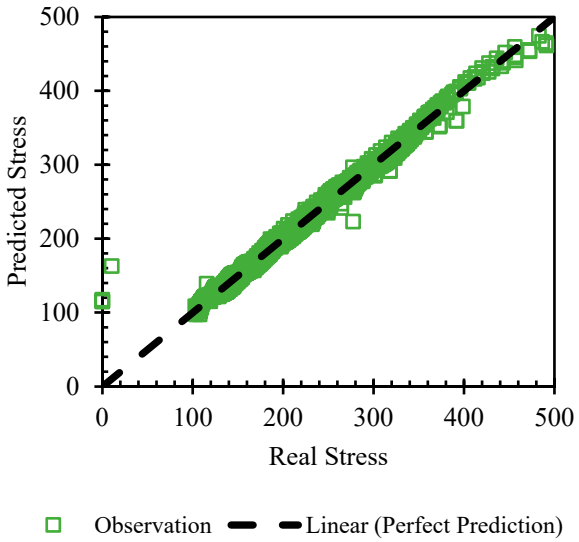


Figure 14. The final training results (SVR).

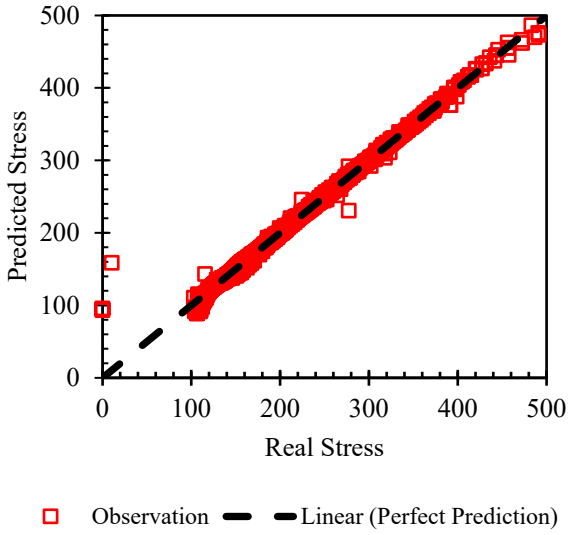


Figure 15. The final training results (GPR).

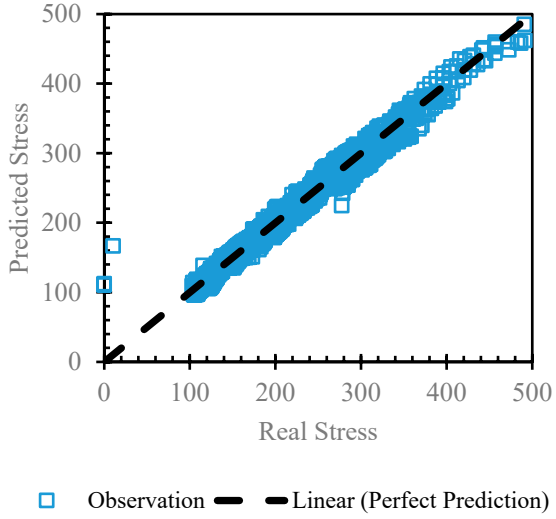


Figure 16. The final training results (SANN).

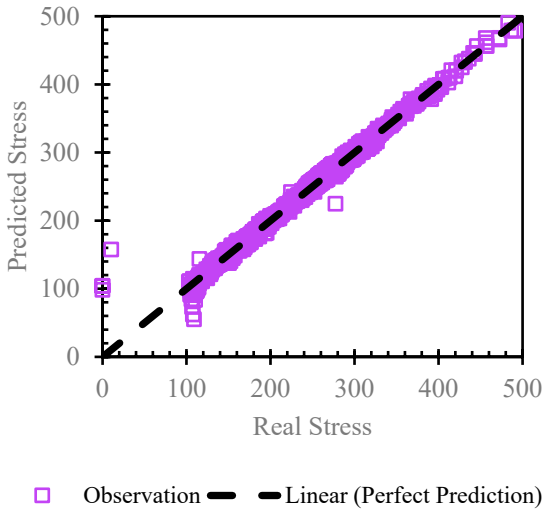


Figure 17. The final training results (DANN).

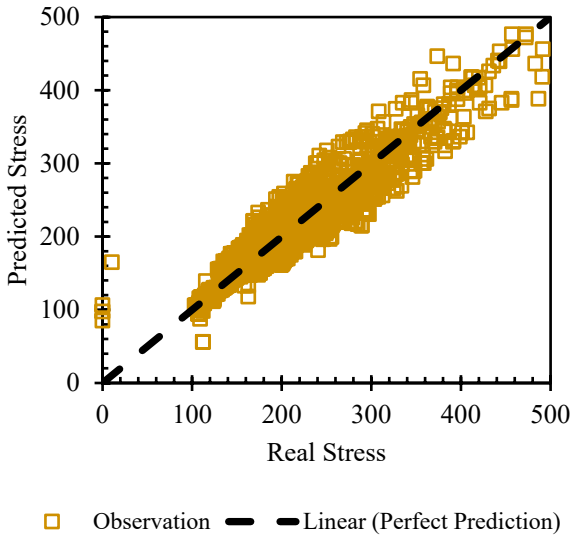
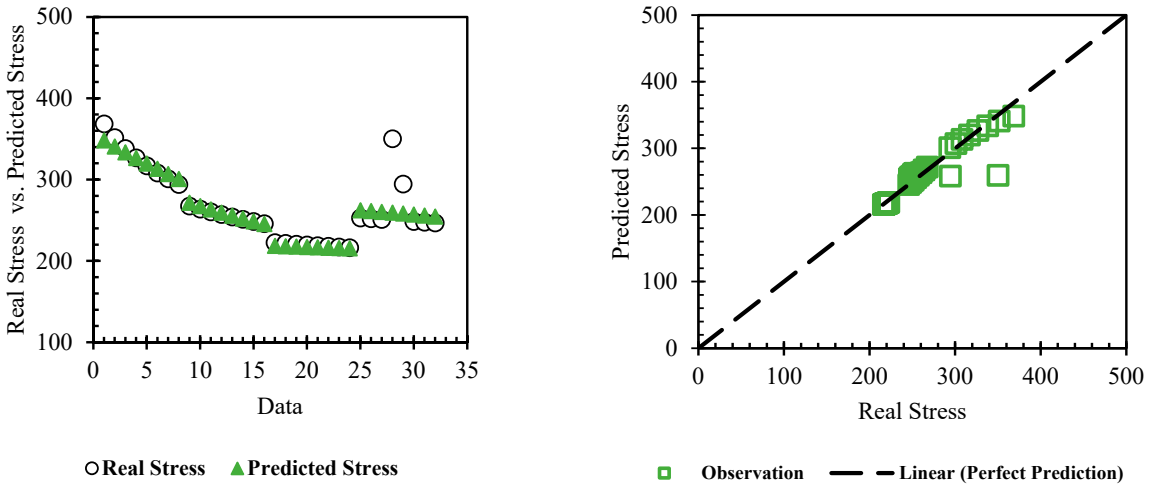


Figure 18. The final training results (LSBoost).

The R^2 parameter is one of the metrics for measuring the stability of the trained algorithm. The R^2 for the SVR model reached 0.98, while the GPR model showed better stability with an R^2 of around 0.99. Both SANN and DANN also provided R^2 values of around 0.99, indicating that the problem's complexity was not very high for ANN. On the other hand, the LSBoost method, with an R^2 of 0.88, did not perform as well compared to the other solutions, as shown in Figure 18.

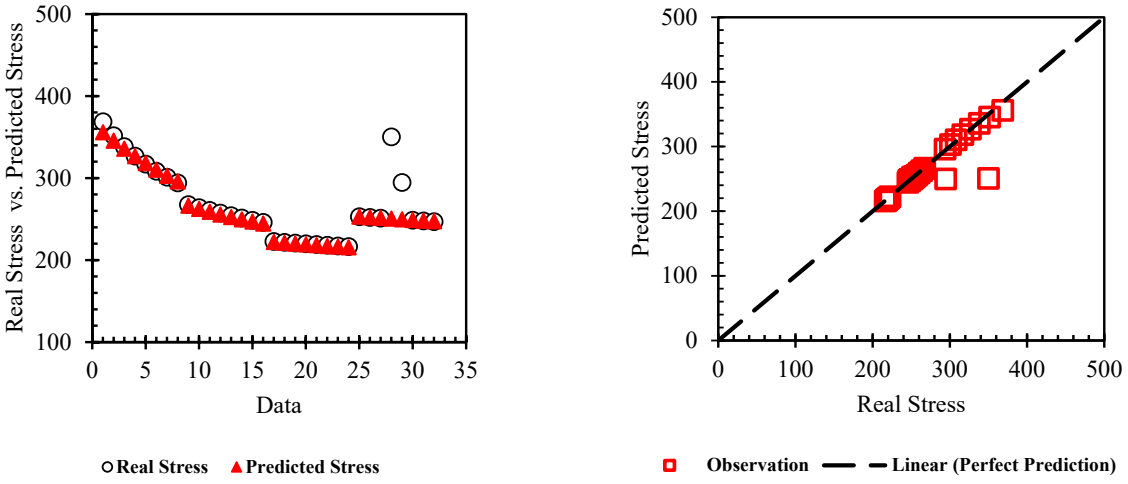
After validating the acceptable hyperparameters for each model and training the models with the provided dataset, the trained models were applied to the testing data. The predicted results were then compared one by one with the actual measurements from outputs of the slab action models in the software.

To validate the prediction models, each model was used on a test dataset in the second phase. The test dataset consisted of 32 datapoints that were separate from the main dataset. It included four different concrete block laying patterns with varying thicknesses and elastic moduli. Figures 19–23 show the final results of applying each algorithm (SVR, GPR, SANN, DANN, and LSBoost) to the test dataset.



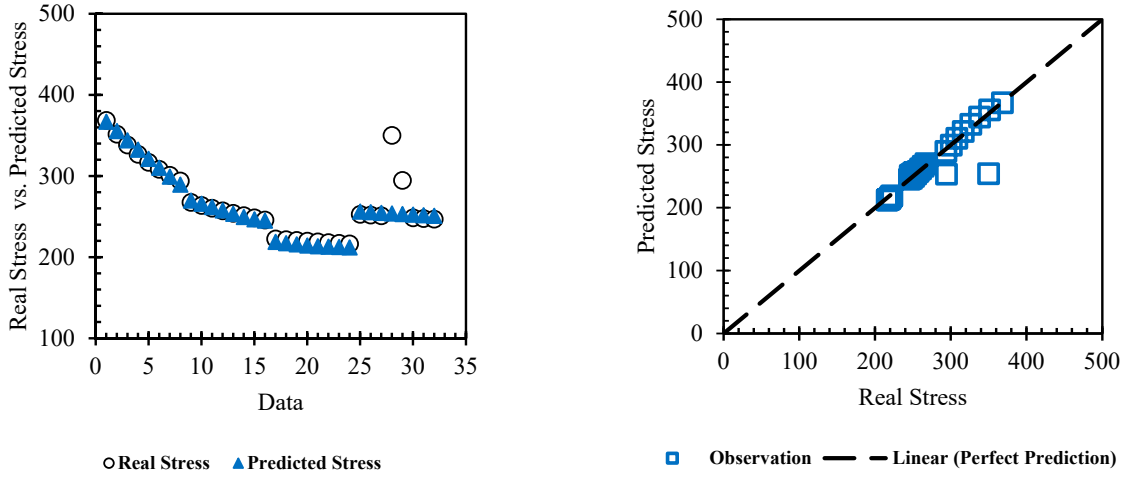
(**a**) Comparison (**b**) Correlation

Figure 19. The final results for test data—SVR Method.



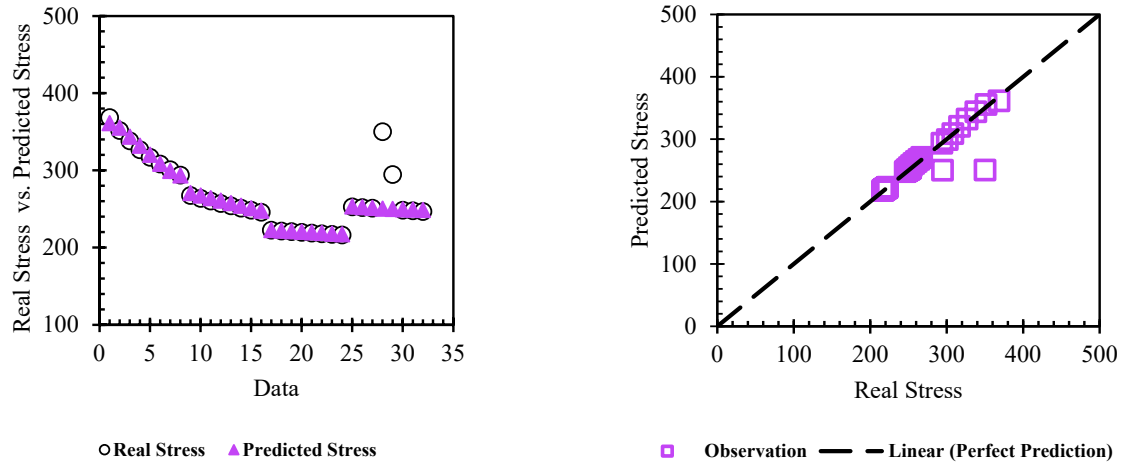
(**a**) Comparison (**b**) Correlation

Figure 20. The final results for test data—GPR Method.



(**a**) Comparison (**b**) Correlation

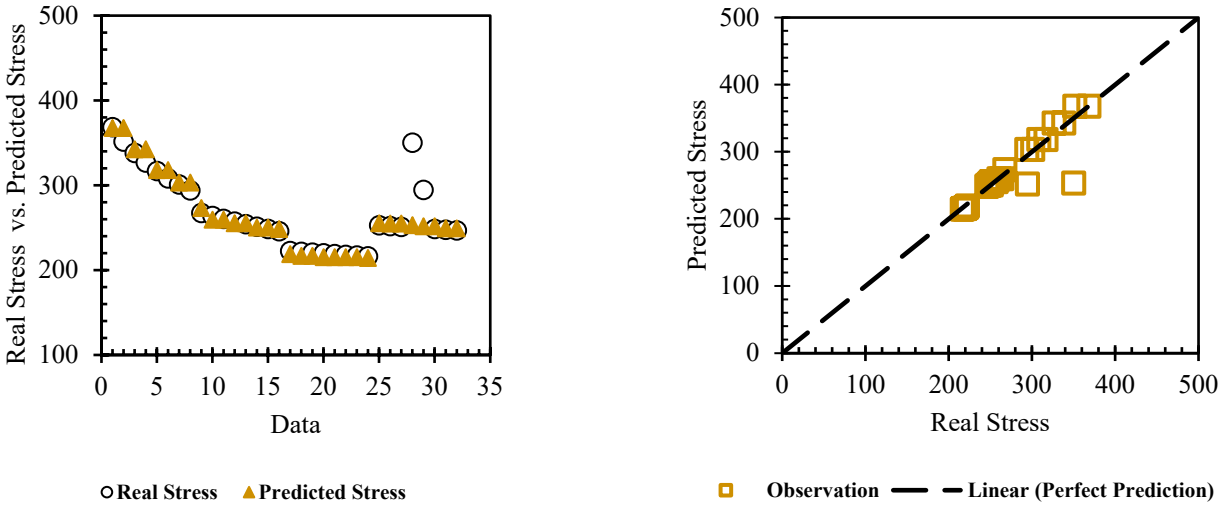
Figure 21. The final results for test data—SANN Method.



(**a**) Comparison (**b**) Correlation

Figure 22. The final results for test data—DANN Method.

The data illustration presents two different models: Figure 19a shows the real and predicted data for a visual comparison of the prediction accuracy, while Figure 19b shows the correlation between the predicted and real data. These metrics provide a clear visualization of the data distribution and accuracy in the test data process.



(**a**) Comparison (**b**) Correlation

Figure 23. The final results for test data—LSBoost Method.

3.4. Accuracy of the Models

The model accuracy metrics for each algorithm are shown in Table 8. It should be noted that these accuracy metrics can be used as indications of the fitness of the models/method and accuracy of the outputs compared with the results yielded from the computer model(s), refer to Figure 4, developed based on the slab action of block pavers and their interactions with joint sand. Obviously, a higher R^2 means that the outputs of the ML models are closer to the outputs of the computer models developed based on slab action and FEM. Moreover, RMSE, MSE, and MAPE indicate errors of the models in different ways. It is clear that lower errors in terms of RMSE, MSE, and MAPE mean a more accurate model or less noise. Since the hidden layers and concepts of the ML approaches adopted in this research are different, it is reasonable to obtain different errors using the same inputs. Additionally, different accuracy metrics can be adopted based on the nature of data and research. Therefore, various errors, e.g., RMSE, MSE, and MAPE, were calculated in this research to provide better insight to the models compared with those that will be developed in the future. Due to the brevity of the paper, only MAPE, which is more popular in the analysis of the accuracy of ML models, is discussed herein. The trends of other errors can be similar, depending on the interpretation of the outputs of ML approaches.

Table 8. Prediction performance in terms of stress for different machine learning models on the training and testing datasets.

Data Set	Accuracy Metrics	SVR	GPR	SANN	DANN	LSBoost
Train	R^2	0.98	0.99	0.97	0.99	0.88
Test	R^2	0.82	0.80	0.81	0.88	0.81
	RMSE	18.37	19.53	19.26	19.44	19.52
	MAE	8.50	6.02	6.48	6.38	8.19
	MAPE	2.85	1.88	2.13	2.05	2.72

All training models except LSBoost have R^2 values higher than 0.97, while the LSBoost model has an R^2 value of 0.88 for predicting stress; however, all the algorithms indicate that they are suitable for application to test the dataset. In the testing dataset, all five models achieved R^2 values above 0.8, which demonstrates that they can produce reasonable results on new input data. The DANN and GPR models outperformed the others in terms of R^2 and MAPE. The DANN model has the best R^2 of about 0.88, while the GPR model has the lowest MAPE of around 1.8%, which indicates that the model has the lowest absolute mean error. Thus, it shows better performance compared to the other models. The SANN and SVR models are in the middle of the range between the best models and LSBoost. The SVR model also provided acceptable results for R^2, around 0.82, and MAPE, about 2.85%, while the SANN model has an R^2 of 0.81 and an MAPE of 2.13%. Although the LSBoost model has an inferior result for R^2 in the training process, it provided an R^2 of about 0.81 and an MAPE of 2.72% in the testing process. However, it should be noted that the lowest performance in the training process could not lead to a robust solution in the testing procedure.

Figure 24 shows a Taylor diagram that compares the performance of various ML models using three key metrics: standard deviation, Pearson correlation, and centered RMSD. These metrics measure the pattern similarity between the predictions of each ML model and the actual observations. An ML model that performs well will demonstrate a high correlation and a low RMSD, while its standard deviation closely matches the actual observations. Therefore, such a model will be positioned closer to the observation point on the diagram, indicating higher accuracy.

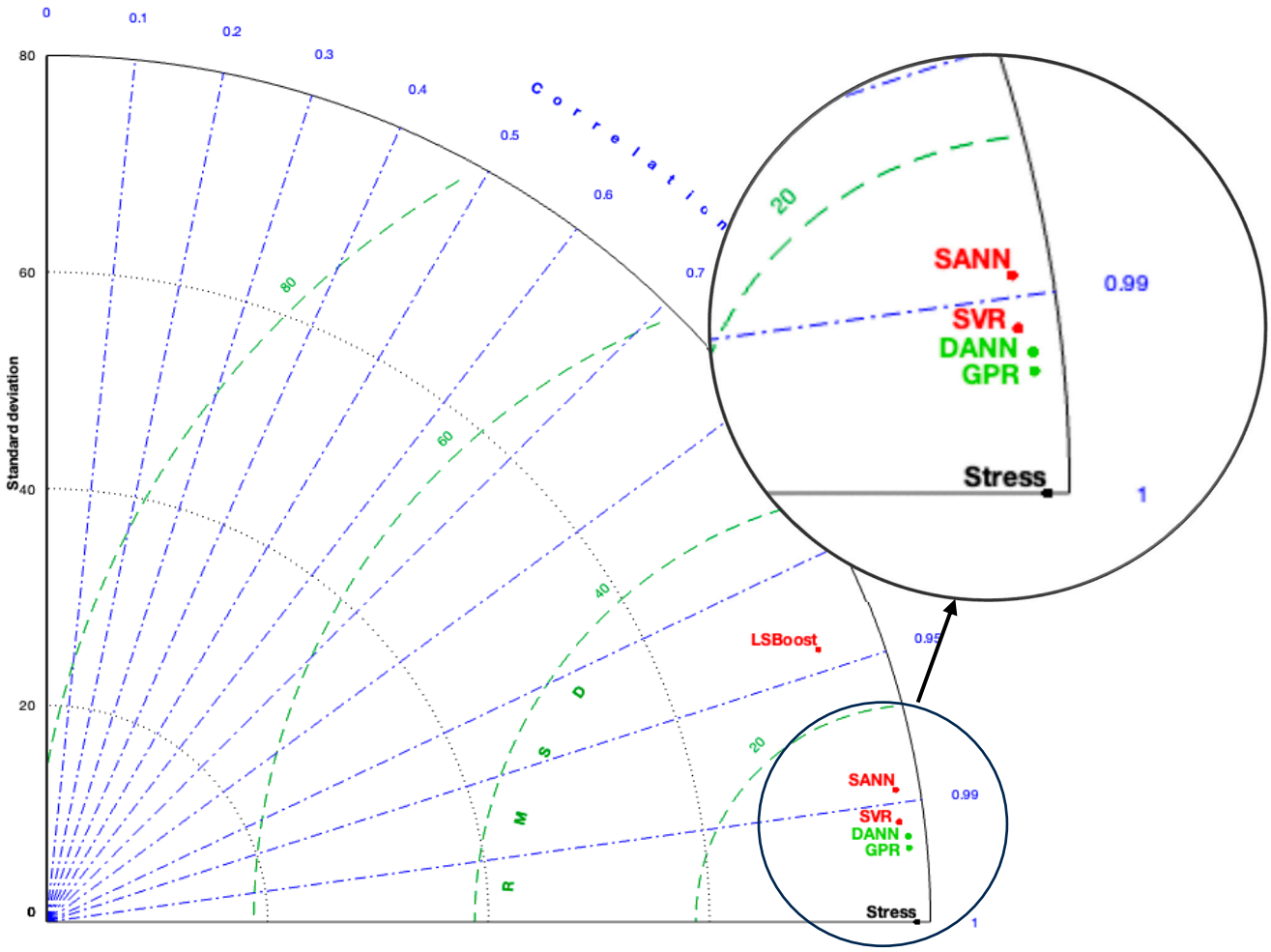


Figure 24. Taylor diagram of different machine learning models, best results highlighted in green.

As illustrated in the Taylor diagram, the DANN and the GPR models perform the best among the algorithms for future investigations. The SVR model also provided reasonable results, making it difficult to omit in any implementation.

Table 9 shows the average accuracy of stress prediction for each algorithm and each type of concrete block pavement compared with the observed data from the test dataset. Although the models for each laying pattern achieved an accuracy above 92%, the GPR and DANN models exhibited slightly better performance in all laying patterns, which can be used as a basis for further studies. In addition, it can be seen that the LSBoost approach showed the lowest accuracy compared with the other approaches, indicating a lower potential for predicting stress, which may depend on the trend of the data, the method of screening, and the data analysis by LSBoost. It should be noted that more data and input variables could result in better training and improved accuracy for LSBoost. Therefore, it is recommended for further research in the future.

Table 9. Prediction performance of different machine learning models on training and testing datasets.

Data Set	SVR	GPR	SANN	DANN	LSBoost
Herringbone	97.9	99.0	98.9	99.2	97.7
Stretcher	99.2	99.4	99.5	98.7	99.1
Parquet	98.9	99.7	97.9	99.7	98.5
Square	92.6	94.4	93.7	94.2	93.9

3.5. Sensitivity Analysis

Figures 25 and 26 illustrate the results of the sensitivity analysis. It should be noted that the effect of block thickness on stress in different block laying patterns was discussed in Figures 9–13; therefore, the effect of block thickness is not shown here. Figure 26 illustrates the effect of changes in laying patterns and elastic modulus (5000, 25,000, and 45,000 MPa) of 100 mm-thick concrete block pavers. The figure clearly shows that the stress under the block layer decreases as elastic moduli increase, which is the same trend observed in all the trends that were tracked correctly identified by all ML methods. However, there is a difference in the outputs of LSboost compared with other models. Lastly, Figure 26 examines the impact of block paving type at two different moduli of elasticity (2500 and 45,000 MPa, the minimum and maximum values in the current dataset, respectively) under a 100 mm-thick CBP. It can be seen that the herringbone laying pattern showed lower stress than other types for both moduli of elasticity, and this trend is correctly tracked by ML methods and the literature. In other words, the block laying patterns modeled based on the slab action phenomenon in FEM showed a trend using ML methods that is consistent with the real performance of CBP.

A noteworthy finding from Figures 25 and 26 is the notable consistency observed between the predicted values produced by the ML models. In other words, this harmonious alignment in stress prediction, achieved through the SVR, GPR, SANN, and DANN models, highlights the models' robustness, precision, and dependability in reflecting real-world scenarios within the specified range.

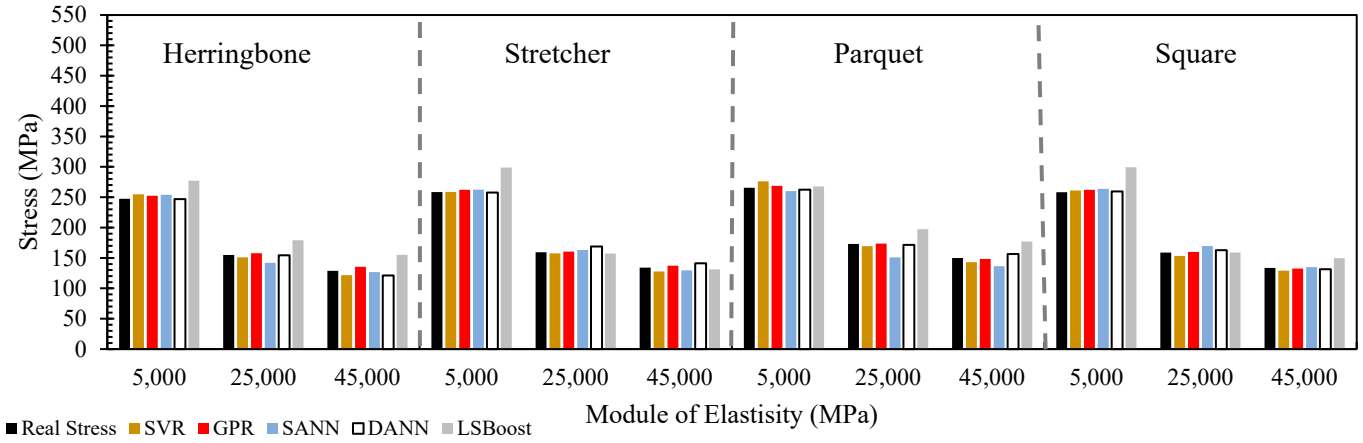


Figure 25. Analysis of the results of input parameters on the stress under different moduli of elasticity for the proposed ML models.

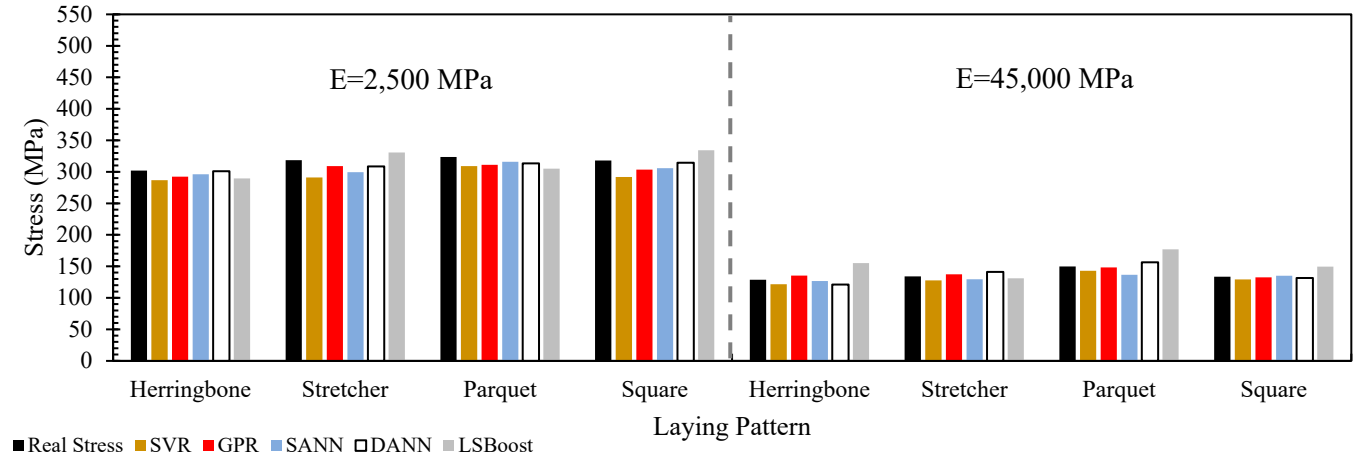
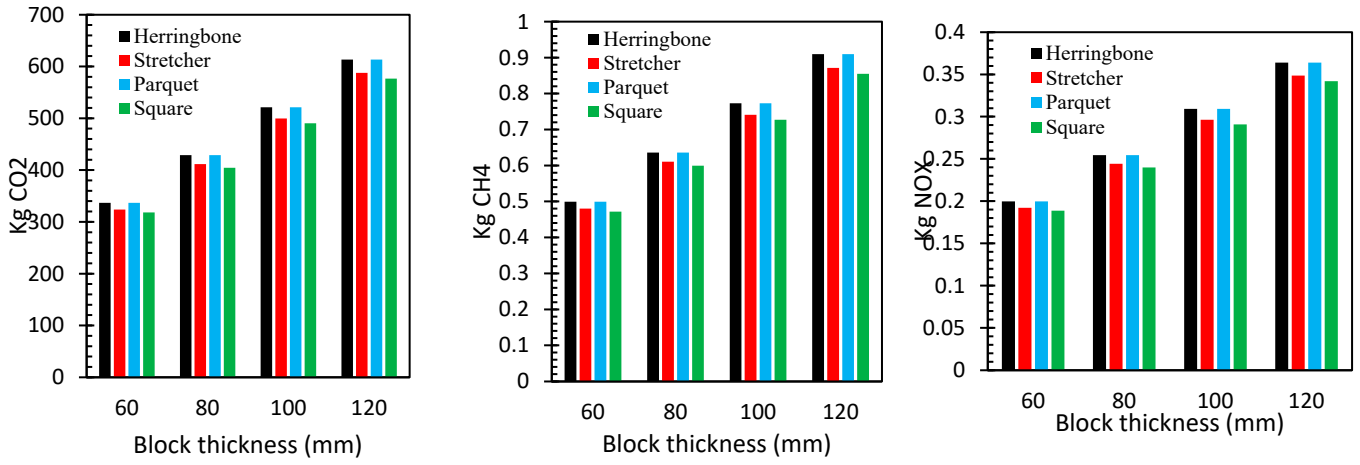


Figure 26. Analysis of the results of input parameters on each block paving pattern under two different moduli of elasticity.

3.6. Analysis of Sustainability

The calculated GHG emission, in terms of CO_2, CH_4, and NO_X, of 2 m × 2 m models in different laying patterns and block thicknesses is shown in Figure 27. The general trend is that total emissions between the different laying patterns with the same block thickness are not significant. It can be seen that the GHG emission of the models increases as the thickness of the block paver increases. It is obvious that the higher thickness of the block paver requires more raw materials, including cement, aggregate particles, and joint sand. Thus, a lower thickness of the block paver may result in a higher environmental sustainability in the block paving layer. The results are comparable with some data provided by Ashokan et al. [83]. However, it should be noted that the energy consumption and GHG emissions of concrete block pavement construction depend on many factors, such as the machinery/technologies used in extracting aggregate or aggregate production, the process used in cement manufacturing, fuel type, the mix design of concrete (water-to-cement ratio, aggregate gradation, and ratio of aggregate to sand), the method/technology of mixing and molding concrete, the types of machinery used for vibrating CBP, and final compaction. Any changes in the variables may result in different outputs. Additionally, it should be noted that all the emissions shown in the figure are only for one elastic modulus of the concrete block paver. For laboratory analyses of the concrete block layer with elastic moduli varying from 2500 MPa to 45,000 MPa with increments of 500 MPa, which results in 85 elastic moduli, massive amounts of raw materials, time, and manpower would be required. It

would be unwise to assign such high effort and budget to such analyses. Additionally, the development of a mix design, vibrating, and curing methods/technology for concrete that results in a specific elastic modulus is based on trial and error. To overcome the challenge, ML approaches and digitalization of the developed models would be helpful. It is worth mentioning that such approaches are just tools for initial engineering judgement based on field experience, construction technology, availability of local materials/paving technology, a highly skilled paving crew, and cost.



(**a**) CO_2 emission (**b**) CH_4 emission (**c**) NO_x emission

Figure 27. GHG emissions.

3.7. Digitalization of CBP Analysis

To produce a user-friendly digital platform to provide a preliminary judgement for engineers, contractors, technologists, and craftsmen, a simple software was developed based on slab action modeling and the ML approach, which can be installed on any electronic device (Figure 1). The user only chooses the block laying pattern, elastic modulus, thickness of the block, and the method of ML (if applicable) to calculate the stress and deflection under 600 KPa. It requires no training or specific data science knowledge. Figure 28 shows the application what was developed based on ML techniques for different block laying patterns and slab action in this study. The application has a minimal and user-friendly UI. It is worth mentioning that the main application of the software is underdeveloped. It should be noted that it is just a tool for facilitating engineering and technical judgement in a time- and cost-effective manner. This fundamental approach and solution can facilitate future software development enhanced by machine learning implementations.

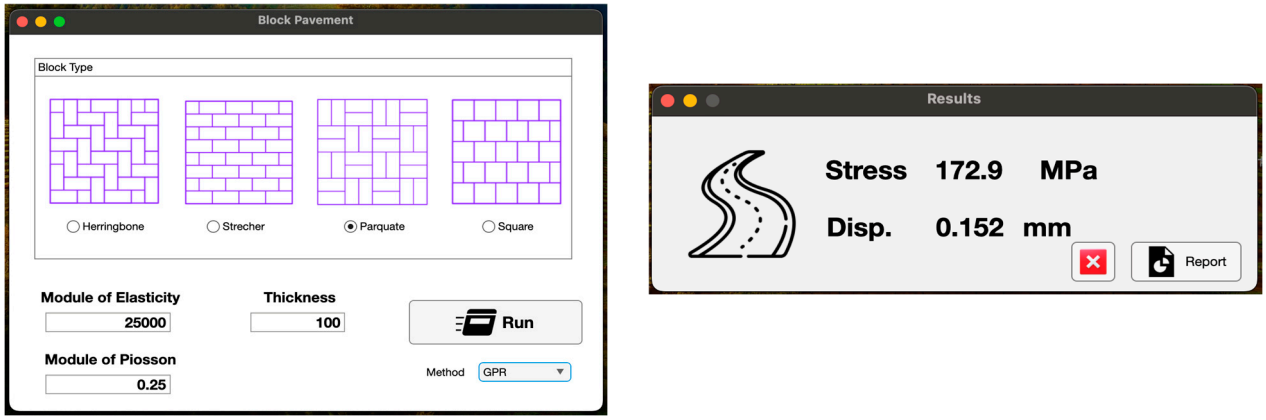


Figure 28. Final UI of the block pavement application.

4. Suggestions for Further Research

The following subjects are recommended for further studies in CBP technology:

- It is interesting to model the dented block pavers using slab action theory. The interaction between pavers in different elastic moduli with joint sand, based on slab action in different laying patterns, remains a gap in knowledge.
- In this research, only a granular base was considered. It is recommended that cement/lime-treated or asphalt-treated bases be considered. As such, further laboratory setups need to be built. It is also recommended that the effect of different subgrade types is included on the stress distribution in CBP.
- In the analysis of sustainability, different industrial fuel types and technologies can be utilized. It is interesting to carry out research on the effect of various industrial fuel types and construction technologies.
- For digitalization, it is suggested to include the models developed based on slab action for different block shapes (dented and rectangular pavers) in different laying patterns, various block thicknesses, and different base materials in machine learning procedures.
- It is also recommended that the role of digitalization (software infrastructure) in design and evaluation be analyzed in terms of life cycle cost and greenhouse gas emissions of the CBP design life.
- The synergistic effects of waste materials in the design/construction of CBP and soft infrastructure, based on machine learning, on sustainability need to be evaluated in further detail.
- It is also suggested to use slab action theory for modeling CBP and machine learning for CBP in airport and port pavements.

5. Conclusions

This study consists of two innovative aspects: modeling the non-homogenous nature of concrete block pavement (CBP), based on the slab action of the block pavers and joint sand, and the development of a machine learning (ML) algorithm for CBP. The non-homogeneous nature of concrete block layer results in those traditional theories applied in the design of asphalt and concrete pavements being unrealistic in CBP. Therefore, it is necessary to include non-homogeneity in the modeling of CBP to model block laying patterns and block shapes. To address this, CBP was modeled based on the slab action of concrete block pavers and joint sand. In this regard, a panel of 2 m $\times$ 2 m with rectangular blocks (200 m $\times$ 100 m), with thicknesses ranging from 60 mm to 120 mm, in different laying patterns was modeled using the finite element method. The model was compared with an analytical and laboratory model, which showed reasonable performance in terms of stress beneath the block layer. In addition, the results of the models showed that a herringbone laying pattern has the lowest stress and deflection in comparison with other laying patterns. Therefore, modeling CBP based on the slab action of concrete block pavers and joint sand in full contact can be a realistic approach, which enables pavement engineers, technologists and researchers to consider different laying patterns and shapes of block pavers in structural design and evaluation. Since it is not easy to model different laying patterns of block pavement, ML approaches were used. In this regard, support vector regression (SVR), Gaussian process regression (GPR), and single-layer artificial neural network (SANN), deep artificial neural network (DANN), and least square boosting (LSBoost) were used to develop the algorithms. The inputs for the models were elastic modulus, 2500 MPa to 45,000 MPa; block thickness, 60 mm to 120 mm; and block laying pattern. Although the block laying pattern is a qualitative input, which is intrinsically different from quantitative inputs like elastic modulus and thickness, the ML models enable pavement technologists and technicians to include such qualitative variables in their models. Therefore, a dataset consisting of 1376 datapoints was created, including 1344 and 32 datapoints for training and testing, respectively. The outputs of the models included stress beneath the block layer and deflection induced through a wheel load of 42 kN.

To evaluate the models, four accuracy metrics—mean absolute percentage error (MAPE), mean absolute error (MAE), root mean squared error (RMSE), and R^2—were used for all the ML models. The statistical analysis through these accuracy metrics showed that the models have very similar performances due to the small differences between the metrics, making it difficult to choose the best model, because all models achieve R^2 values above 0.8, indicating satisfactory results. Thus, a Taylor diagram was used to select the best model, which revealed that the GPR and DANN models were more accurate than the others. However, the outputs of GPR showed slightly better performance. Therefore, GPR can be adopted for further development in the future.

Although the model developed based on slab action showed promising results, there are some limitations. Only rectangular blocks on the granular base were modeled. It is recommended to model CBP using dented blocks in different laying patterns and use various machine learning methodologies for further studies. It should be noted that slab action can be used for modeling CBP used in other infrastructure assets such as airports, ports, and stacking container yards.

The analysis of sustainability showed that the GHG emissions for different block laying patterns with similar block thicknesses are similar, even though the GHG emissions increase as the thickness of the block paver increases due to higher raw material consumption and more concrete material for vibrating, pressing, and curing.

Based on the ML models, a simple, user-friendly software was developed to digitalize in situ evaluation of CBP for initial judgement with minimum training for engineers, craftsmen, technologists, and researchers. This software is merely a simple tool to facilitate engineering judgement. It is not a substitute for sound analysis through laboratory testing, field investigation, and engineering experience. In other words, such a tool can facilitate engineering judgement through resource- and time-saving, which results in sustainability through digital transformation. Therefore, it is a tool for in situ judgment, which paves the way for the digital transformation of existing ad hoc methods of CBP design toward sophisticated computer packages on the basis of ML approaches. It is also a resource- and time-saving approach, which significantly decreases the carbon footprint of laboratory efforts and increases sustainability in pavement construction.

Author Contributions: Conceptualization A.J. and P.N., Methodology: A.J., R.H. and P.N.; Software: M.D.A. and P.N.; Visualization: M.D.A. and M.G.; Validation: B.G. and P.N.; Formal analysis: B.G.; Investigation: M.D.A.; Resources: M.D.A. and P.N.; Data curation: M.G., Writing—original draft preparation: A.J., M.D.A. and P.N.; Writing—review and editing: A.J. and R.H.; Supervision: A.J.; Project administration: A.J. All authors have read and agreed to the published version of the manuscript.

Funding: This research received no external funding.

Institutional Review Board Statement: Not applicable.

Informed Consent Statement: Informed consent was obtained from all subjects involved in the study.

Data Availability Statement: The original contributions presented in the study are included in the article, further inquiries can be directed to the corresponding author.

Conflicts of Interest: The authors declare no conflicts of interest.

References

1. Shackel, B.; Pearson, A.; Holt, W. A Survey of Australian Container Port Pavements Surfaced with Concrete Segmental Paving. In Proceedings of the 7th International Conference on Concrete Block Paving, Sun City, South Africa, 12–15 October 2003.
2. Shackel, B. *Design and Construction of Interlocking Concrete Block Pavements*; Elsevier Applied Science: Amsterdam, The Netherlands, 1990.
3. Knapton, J.; Smith, D.R. The North American Port Pavement Design Manual. In Proceedings of the 3rd International Workshop on Concrete Block Paving, Cartagena de Indias, Colombia, 10–13 May 1998.
4. Jamshidi, A.; White, G. Summary of Strategies of the Analysis and Structural Design of Concrete Block Pavements. In Proceedings of the 12th International Conference on Concrete Block Paving, Seoul, Republic of Korea, 16–19 October 2018.
5. Potter, D.W.; Donald, G.S. Revision of NAASRA Interim Guide to Pavement Thickness Design. *Aust. Road Res.* **1985**, *15*, 106–112.

6. Shackel, B. The Analysis and Design of Concrete Block Paving Subject to Road Traffic and Heavy Industrial Loading Traffic. In Proceedings of the 2nd International Workshop on Concrete Block Paving, Delft, The Netherlands, 10–12 April 1984.
7. Nejad, F.M.; Shadravan, M.R. A Study on Behavior of Block Pavement Using 3D Finite Element Method. *Comput. Methods Civ. Eng.* **2010**, *1*, 65–71.
8. Nejad, F.M. Finite Element Analysis on Concrete Block Paving. In Proceedings of the 7th International Conference on Concrete Block Paving, Sun City, South Africa, 12–15 October 2003.
9. Hassani, A.; Jamshidi, A. Modeling and Structural Design of a Concrete Block Pavement System. In Proceedings of the 8th International Conference on Concrete Block Paving, San Francisco, CA, USA, 6–9 November 2006.
10. Shackel, B. Computer-Based Mechanistic Methods for Concrete Block Pavement Design. In Proceedings of the 6th International Conference on Concrete Block Paving, Tokyo, Japan, 6–9 November 2000.
11. Rahman, M.M.; Beecham, S.; McIntyre, E. A New Approach to the Mechanistic Design and Analysis of Concrete Block Pavement. In Proceedings of the 12th International Conference on Concrete Block Paving, Seoul, Republic of Korea, 16–19 October 2018.
12. Sun, L. Design Theory and Method of Interlocking Concrete Block Paving for Port Areas. In Proceedings of the 5th International Conference on Concrete Block Paving, Delft, The Netherlands, 23–27 June 1996.
13. Ascher, D.; Lerch, T.; Oeser, M.; Wellner, F. 3D-FEM Simulation of Concrete Block Pavements. In Proceedings of the 8th International Conference on Concrete Block Paving, San Francisco, CA, USA, 6–9 November 2006.
14. Hurez, M. Open Systems: Co-ordination Conventions in Developing Open Building Systems-Computer Software Analysis with the Support of the French Ministry of Building Initiatives. *Batim. Int. Build. Res. Pract.* **1988**, *16*, 356–362. [CrossRef]
15. Nishizawa, T. A Tool for Structural Analysis of Block Pavements Based on 3DFEM. In Proceedings of the 7th International Conference on Concrete Block Paving, Sun City, South Africa, 12–15 October 2003.
16. Arjun Siva Rathan, R.T.; Sunitha, V. Development of Design Procedure for Interlocking Concrete Block Pavement. *Int. J. Pavement Eng.* **2022**, *23*, 5015–5029. [CrossRef]
17. Huurman, M.; Houben, L.J.M.; Geense, C.W.A.; der Vring, J.J.M. The Upgraded Dutch Design Method for Concrete Block Road Pavements. In Proceedings of the 7th International Conference on Concrete Block Paving, Sun City, South Africa, 12–15 October 2003.
18. Mampearachchi, W.K.; Gunarathna, W.P.H. Finite-Element Model Approach to Determine Support Conditions and Effective Layout for Concrete Block Paving. *J. Mater. Civ. Eng.* **2010**, *22*, 1139–1147. [CrossRef]
19. Drenth, K. ELMOD 6: The Design and Structural Evaluation Package for Road, Airport and Industrial Pavements. In Proceedings of the 8th International Conference on Concrete Block Paving, San Francisco, CA, USA, 6–9 November 2006.
20. Knapton, J.; Morrell, D. Heavy Duty Pavements: The Structural Design of Heavy Duty Pavements for Ports and Other Industries. *Landscape* **2010**, *44*, 1422.
21. Taheri, V.; Fakhri, M.; Hayati, P. Evaluation of Airfield Concrete Block Pavements Based on 3-D Modelling and Plate Loading Test. *Constr. Build. Mater.* **2021**, *280*, 122441. [CrossRef]
22. Lin, W.; Cho, Y.; Kim, I.T. Development of Deflection Prediction Model for Concrete Block Pavement Considering the Block Shapes and Construction Patterns. *Adv. Mater. Sci. Eng.* **2016**, *2016*, 5126436. [CrossRef]
23. Habib, M.; Okayli, M. Evaluating the Sensitivity of Machine Learning Models to Data Preprocessing Technique in Concrete Compressive Strength Estimation. *Arab. J. Sci. Eng.* **2024**, *49*, 1–19. [CrossRef]
24. Sah, A.K.; Hong, Y.-M. Performance Comparison of Machine Learning Models for Concrete Compressive Strength Prediction. *Materials* **2024**, *17*, 2075. [CrossRef]
25. Beskopylny, A.N.; Stel'makh, S.A.; Shcherban', E.M.; Mailyan, L.R.; Meskhi, B.; Razveeva, I.; Chernil'nik, A.; Beskopylny, N. Concrete Strength Prediction Using Machine Learning Methods CatBoost, k-Nearest Neighbors, Support Vector Regression. *Appl. Sci.* **2022**, *12*, 10864. [CrossRef]
26. Denu, E.G.; Cho, Y.-H. Block Pavement and Distress Segmentation Using Deep Learning Models. *Innov. Infrastruct. Solut.* **2024**, *9*, 244. [CrossRef]
27. Jung, D.; Lee, J.; Baek, C.; An, D.; Yang, S. Predicting Concrete Pavement Condition for Sustainable Management: Unveiling the Development of Distresses through Machine Learning. *Sustainability* **2024**, *16*, 573. [CrossRef]
28. Wang, X.; Chin, C.; Xia, J. Material Characterization for Sustainable Concrete Paving Blocks. *Appl. Sci.* **2019**, *9*, 1197. [CrossRef]
29. Jamshidi, A.; Kurumisawa, K.; Nawa, T.; Igarashi, T. Performance of Pavements Incorporating Waste Glass: The Current State-of-the-Art. *Renew. Sustain. Energy Rev.* **2016**, *64*, 211–236. [CrossRef]
30. Iftikhar, B.; Alih, S.C.; Vafaei, M.; Javed, M.F.; Ali, M.; Gamil, Y.; Rehman, M.F. A Machine Learning-Based Genetic Programming Approach for the Sustainable Production of Plastic Sand Paver Blocks. *J. Mater. Res. Technol.* **2023**, *25*, 5705–5719. [CrossRef]
31. Qin, Y.; He, Y.; Hiller, J.E.; Mei, G. A New Water-Retaining Paver Block for Reducing Runoff and Cooling Pavement. *J. Clean. Prod.* **2018**, *199*, 948–956. [CrossRef]
32. Luo, W.; Liu, S.; Hu, Y.; Hu, D.; Kow, K.-W.; Pang, C.; Li, B. Sustainable Reuse of Excavated Soil and Recycled Concrete Aggregate in Manufacturing Concrete Blocks. *Constr. Build. Mater.* **2022**, *342*, 127917. [CrossRef]
33. Jamshidi, A.; Kurumisawa, K.; Nawa, T.; Jize, M.; White, G. Performance of Pavements Incorporating Industrial Byproducts: A State-of-the-Art Study. *J. Clean. Prod.* **2017**, *164*, 367–388. [CrossRef]
34. Gan, V.J.L.; Lo, I.M.C.; Ma, J.; Tse, K.T.; Cheng, J.C.P.; Chan, C.M. Simulation Optimisation Towards Energy Efficient Green Buildings: Current Status and Tuture Trends. *J. Clean. Prod.* **2020**, *254*, 120012. [CrossRef]

35. Shoval, S.; Rosenfeld, Y.; Navon, R. Automatic Palletizing of Concrete Pavement Blocks: An Algorithm for Near-Optimal Assembly. *Comput. Aided Civ. Eng.* **2001**, *16*, 180–187. [CrossRef]
36. Hengl, H.L.; Kluger-Eigl, W.; Lukacevic, M.; Blab, R.; Füssl, J. Horizontal Deformation Resistance of Paving Block Superstructures–Influence of Paving Block Type, Laying Pattern, and Joint Behaviour. *Int. J. Pavement Res. Technol.* **2018**, *19*, 1575–1594. [CrossRef]
37. Shahrokhishahraki, M.; Malekpour, M.; Mirvalad, S.; Faraone, G. Machine Learning Predictions for Optimal Cement Content in Sustainable Concrete Constructions. *J. Build. Eng.* **2024**, *82*, 108160. [CrossRef]
38. Asadi, B.; Hajj, R. Prediction of Asphalt Binder Elastic Recovery Using Tree-Based Ensemble Bagging and Boosting Models. *Constr. Build. Mater.* **2024**, *410*, 134154. [CrossRef]
39. Al-Sabaeei, A.M.; Souliman, M.I.; Jagadeesh, A. Smartphone Applications for Pavement Condition Monitoring: A Review. *Constr. Build. Mater.* **2024**, *410*, 134207. [CrossRef]
40. Li, J.; Zhang, Z.; Wang, X. Performance-Oriented Road Structure and Material Design Method Based on Enhanced XGBoost Algorithm. *Int. J. Pavement Eng.* **2024**, *25*. [CrossRef]
41. Chen, X.; Dong, Q.; Dong, S. Evaluation and Prediction of Pavement Deflection Parameters Based on Machine Learning Methods. *Buildings* **2022**, *12*, 1928. [CrossRef]
42. Ghorbani, B.; Arulrajah, A.; Narsilio, G.; Horpibulsuk, S. Experimental Investigation and Modelling the Deformation Properties of Demolition Wastes Subjected to Freeze–Thaw Cycles Using ANN and SVR. *Constr. Build. Mater.* **2020**, *258*, 119688. [CrossRef]
43. Chou, J.-S.; Pham, A.-D. Smart Artificial Firefly Colony Algorithm-Based Support Vector Regression for Enhanced Forecasting in Civil Engineering. *Comput.-Aided Civ. Infrastruct. Eng.* **2015**, *30*, 715–732. [CrossRef]
44. Debnath, P.; Dey, A.K. Prediction of Bearing Capacity of Geogrid-Reinforced Stone Columns Using Support Vector Regression. *Int. J. Geomech.* **2018**, *18*, 1–15. [CrossRef]
45. Kardani, N.; Zhou, A.; Nazem, M.; Shen, S.-L. Estimation of Bearing Capacity of Piles in Cohesionless Soil Using Optimised Machine Learning Approaches. *Geotech. Geol. Eng.* **2020**, *38*, 2271–2291. [CrossRef]
46. Sheibani, M.; Ou, G. The Development of Gaussian Process Regression for Effective Regional Post-earthquake Building Damage Inference. *Comput.-Aided Civ. Infrastruct. Eng.* **2021**, *36*, 264–288. [CrossRef]
47. Okazaki, Y.; Okazaki, S.; Asamoto, S.; Chun, P. Applicability of Machine Learning to a Crack Model in Concrete Bridges. *Comput.-Aided Civ. Infrastruct. Eng.* **2020**, *35*, 775–792. [CrossRef]
48. Nguyen, T.; Kashani, A.; Ngo, T.; Bordas, S. Deep Neural Network with High-order Neuron for the Prediction of Foamed Concrete Strength. *Comput.-Aided Civ. Infrastruct. Eng.* **2019**, *34*, 316–332. [CrossRef]
49. Lam, H.-F.; Yuen, K.-V.; Beck, J.L. Structural Health Monitoring via Measured Ritz Vectors Utilizing Artificial Neural Networks. *Comput.-Aided Civ. Infrastruct. Eng.* **2006**, *21*, 232–241. [CrossRef]
50. Achieng, K.O. Modelling of Soil Moisture Retention Curve Using Machine Learning Techniques: Artificial and Deep Neural Networks vs Support Vector Regression Models. *Comput. Geosci.* **2019**, *133*, 104320. [CrossRef]
51. Han, H.; Choi, C.; Kim, J.; Morrison, R.R.; Jung, J.; Kim, H.S. Multiple-Depth Soil Moisture Estimates Using Artificial Neural Network and Long Short-Term Memory Models. *Water* **2021**, *13*, 2584. [CrossRef]
52. Lagaros, N.D. Artificial Neural Networks Applied in Civil Engineering. *Appl. Sci.* **2023**, *13*, 1131. [CrossRef]
53. Keshavarz, Z.; Torkian, H. Application of ANN and ANFIS Models in Determining Compressive Strength of Concrete. *J. Soft Comput. Civ. Eng.* **2018**, *2*, 62–70. [CrossRef]
54. Alajmi, M.S.; Almeshal, A.M. Least Squares Boosting Ensemble and Quantum-Behaved Particle Swarm Optimization for Predicting the Surface Roughness in Face Milling Process of Aluminum Material. *Appl. Sci.* **2021**, *11*, 2126. [CrossRef]
55. Mei, L.; Wang, Q. Structural Optimization in Civil Engineering: A Literature Review. *Buildings* **2021**, *11*, 66. [CrossRef]
56. Plevris, V.; Solorzano, G.; Bakas, N.; Seghier, M.B. Investigation of Performance Metrics in Regression Analysis and Machine Learning-Based Prediction Models. In Proceedings of the 8th European Congress on Computational Methods in Applied Sciences and Engineering, Oslo, Norway, 5 June 2022.
57. Botchkarev, A. A New Typology Design of Performance Metrics to Measure Errors in Machine Learning Regression Algorithms. *Interdiscip. J. Inf. Knowl. Manag.* **2019**, *14*, 045–076. [CrossRef] [PubMed]
58. Chicco, D.; Warrens, M.J.; Jurman, G. The Coefficient of Determination R-Squared Is More Informative than SMAPE, MAE, MAPE, MSE and RMSE in Regression Analysis Evaluation. *PeerJ Comput. Sci.* **2021**, *7*, e623. [CrossRef]
59. Taylor, K.E. Summarizing Multiple Aspects of Model Performance in a Single Diagram. *J. Geophys. Res. Atmos.* **2001**, *106*, 7183–7192. [CrossRef]
60. AzariJafari, H.; Yahia, A.; Ben Amor, M. Life Cycle Assessment of Pavements: Reviewing Research Challenges and Opportunities. *J. Clean. Prod.* **2016**, *112*, 2187–2197. [CrossRef]
61. Trunzo, G.; Moretti, L.; D'Andrea, A. Life Cycle Analysis of Road Construction and Use. *Sustainability* **2019**, *11*, 377. [CrossRef]
62. Ivel, J.; Watson, R.; Abbassi, B.; Abu-Hamatteh, Z.S. Life Cycle Analysis of Concrete and Asphalt Used in Road Pavements. *Environ. Eng. Res.* **2019**, *25*, 52–61. [CrossRef]
63. Goyal, H.; Kumar, R.; Mondal, P. Life Cycle Analysis of Paver Block Production Using Waste Plastics: Comparative Assessment with Concrete Paver Blocks. *J. Clean. Prod.* **2023**, *402*, 136857. [CrossRef]
64. Chan, S.; Lane, B.; Kazmierowski, T.; Lee, W. Pavement Preservation: A Solution for Sustainability. *Transp. Res. Rec.* **2011**, *2235*, 36–42. [CrossRef]

65. Dos Santos, J.M.O.; Thyagarajan, S.; Keijzer, E.; Flores, R.F.; Flintsch, G. Comparison of Life-Cycle Assessment Tools for Road Pavement Infrastructure. *Transp. Res. Rec.* **2017**, *2646*, 28–38. [CrossRef]
66. Jullien, A.; Dauvergne, M.; Proust, C. Road LCA: The Dedicated ECORCE Tool and Database. *Int. J. Life Cycle Assess* **2015**, *20*, 655–670. [CrossRef]
67. Lippiatt, B.C. *BEES 4.0: Building for Environmental and Economic Sustainability. Technical Manual and User Guide*; NIST: Gaithersburg, MD, USA, 2007.
68. National Crushed Stone Association. *Flexible Pavement Cost Estimating: Inflation/Energy Effects*; National Crushed Stone Association (NCSA): Alexandria, VA, USA, 1977.
69. Zapata, P.; Gambatese, J.A. Energy Consumption of Asphalt and Reinforced Concrete Pavement Materials and Construction. *J. Infrastruct. Syst.* **2005**, *11*, 9–20. [CrossRef]
70. Jamshidi, A.; Kurumisawa, K.; Nawa, T.; Samali, B.; Igarashi, T. Evaluation of Energy Requirement and Greenhouse Gas Emission of Concrete Heavy-Duty Pavements Incorporating High Volume of Industrial by-Products. *J. Clean. Prod.* **2017**, *166*, 1507–1520. [CrossRef]
71. Garces, J.I.T.; Tan, R.R.; Beltran, A.B.; Ongpeng, J.M.C.; Promentilla, M.A.B. Environmental Life Cycle Assessment of Alkali-Activated Material with Different Mix Designs and Self-Healing Agents. *Chem. Eng. Trans.* **2021**, *88*, 835–840. [CrossRef]
72. Energy Conversion Calculators—U.S. Energy Information Administration (EIA). Available online: https://www.eia.gov/energyexplained/units-and-calculators/energy-conversion-calculators.php (accessed on 2 July 2024).
73. DEFRA. *Guidelines to Defra/DECC's GHG Conversion Factors for Company Reporting (Version 1.2.1)*; Department for Environment, Food and Rural Affairs: London, UK, 2010.
74. Shackel, B. An Experimental Investigation of the Response of Interlocking Concrete Block Pavements to Simulated Traffic Loading. In Proceedings of the Australian Road Research Board Conference Proceeding, Sydney, Australia, 29 January 1979.
75. Eisenmann, J.; Leykauf, G. Design of Concrete Block Pavements in FRG. In Proceedings of the 1st Workshop on Concrete Block Paving, Melbourne, Australia, 1–2 September 1986.
76. Jamshidi, A.; Kurumisawa, K.; White, G.; Nishizawa, T.; Igarashi, T.; Nawa, T.; Mao, J. State-of-the-Art of Interlocking Concrete Block Pavement Technology in Japan as a Post-Modern Pavement. *Constr. Build. Mater.* **2019**, *200*, 713–755. [CrossRef]
77. Algin, H.M. Interlock Mechanism of Concrete Block Pavements. *J. Transp. Eng.* **2007**, *133*, 318–326. [CrossRef]
78. Lin, W.; Kwon, S.A.; Cho, Y.-H. Load Transfer Efficiency Evaluation in Block Pavements Relative to Block Configurations. In Proceedings of the 12th International Conference on Concrete Block Pavement, Seoul, Republic of Korea, 16–19 October 2018.
79. Lin, W.; Kwon, S.A.; Cho, Y.-H. The Performance of Interlocking Concrete Block Pavements with Various Surface Structures. In Proceedings of the 12th International Conference on Concrete Block Paving, Seoul, Republic of Korea, 16–19 October 2018.
80. Panda, B.C.; Ghosh, A.K. Structural Behavior of Concrete Block Paving. II: Concrete Blocks. *J. Transp. Eng.* **2002**, *128*, 130–135. [CrossRef]
81. Lin, W.; Kim, D.; Ryu, S.; Hao, H.; Ge, Y.-E.; Cho, Y.-H. Evaluation of the Load Dissipation Behavior of Concrete Block Pavements with Various Block Shapes and Construction Patterns. *J. Mater. Civ. Eng.* **2018**, *30*, 04017291. [CrossRef]
82. Wang, H.; Li, M.; Szary, P.; Hu, X. Structural Assessment of Asphalt Pavement Condition Using Backcalculated Modulus and Field Data. *Constr. Build. Mater.* **2019**, *211*, 943–951. [CrossRef]
83. Ashokan, A.; Jaganathan, S.; Rajendran, S.; Dhairiyasamy, R. Analysis of Environmental Performance Indicators for Concrete Block Manufacturing: Embodied Energy, CO_2 Emissions, and Water Consumption. *Environ. Sci. Pollut. Res.* **2024**, *31*, 8842–8862. [CrossRef]

Disclaimer/Publisher's Note: The statements, opinions and data contained in all publications are solely those of the individual author(s) and contributor(s) and not of MDPI and/or the editor(s). MDPI and/or the editor(s) disclaim responsibility for any injury to people or property resulting from any ideas, methods, instructions or products referred to in the content.